Transgenic mice expressing human alpha-synuclein in noradrenergic neurons develop locus coeruleus pathology and non-motor features of Parkinson's disease

Butkovich LM[1], Houser MC[1], Chalermpalanupap T[1,2], Porter-Stransky KA[2,3], Iannitelli AF[1,2], Boles JS[4], Lloyd GM[4], Coomes AS[4], Eidson LN[1], De Sousa Rodrigues ME[1], Oliver DL[1], Kelly SD[1], Chang J[1], Bengoa-Vergniory N[5], Wade-Martins R[5], Giasson BI[4], Joers V[4], Weinshenker D[2], Tansey MG[4,6]

[1] Laney Graduate School, Emory University, 30322
[2] Department of Human Genetics, Emory School of Medicine, 30322
[3] Department of Biomedical Sciences, Western Michigan University Homer Stryker M.D. School of Medicine, 49008
[4] Department of Neuroscience and Center for Translational Research in Neurodegenerative Disease, University of Florida College of Medicine, 32610
[5] Oxford Parkinson's Disease Centre, Department of Physiology, Anatomy and Genetics, University of Oxford, UK OX1 3QX
[6] Susan and Normal Fixel Chair in Parkinson's Disease, Normal Fixel Institute for Neurological Diseases, University of Florida Health, 32610

Contact:
Malú Gámez Tansey, PhD
Department of Neuroscience
University of Florida College of Medicine
1149 Newell Drive, L5-101B
Gainesville, FL 32610
mgtansey@ufl.edu

Key words: Parkinson's disease, α-synuclein, locus coeruleus, aging, norepinephrine

Acknowledgements
We thank Terina Martinez, Tim Sampson, and the Tansey, Weinshenker, and Giasson labs for useful discussions. This work was supported by NIH/NINDS 5F31 NS098673 (LB), NIH/NINDS F32 NS098615 (KP), NIH/NINDS 1R01 NS102306 (DW), NIH/NIA 1RF1 AG047667 (DW), NIH/NIA 1R01AG061175 (DW), NIH/NINDS 1R01 NS100876 (BG), NIH/NIA 1R01 AG057247 (MGT), NIH/NINDS 5R01 NS092122 (MGT), NIH/NIA 3RF1 AG051514-01 (MGT), and the Norman Fixel Institute for Neurological Diseases (MGT). This research project was also supported in part by the Emory University Integrated Cellular Imaging Microscopy Core, by the Rodent Behavioral Core (RBC), which is subsidized by the Emory University School of Medicine and is one of the Emory Integrated Core Facilities. Additional support was provided by the Emory Neuroscience NINDS Core Facilities P30NS055077. Further support was provided by the Georgia Clinical & Translational Science Alliance of the National Institutes of Health under Award Number

UL1TR002378. This study was supported in part by the Emory HPLC Bioanalytical Core (EHBC), which was supported by the Department of Pharmacology, Emory University School of Medicine and the Georgia Clinical & Translational Science Alliance of the National Institutes of Health under Award Number UL1TR002378. The content is solely the responsibility of the authors and does not necessarily reflect the official views of the National Institutes of Health.

Word count: Abstract =186; Introduction =598; Discussion =1573

Abstract

Degeneration of locus coeruleus (LC) neurons and dysregulation of noradrenergic signaling are ubiquitous features of Parkinson's disease (PD). The LC is among the first brain regions affected by α-synuclein (asyn) pathology, yet how asyn affects these neurons remains unclear. LC-derived norepinephrine (NE) can stimulate neuroprotective mechanisms and modulate immune cells, while dysregulation of NE neurotransmission may exacerbate disease progression, particularly non-motor symptoms, and contribute to the chronic neuroinflammation associated with PD pathology. Although transgenic mice overexpressing asyn have previously been developed, transgene expression is usually driven by pan-neuronal promoters and thus has not been selectively targeted to LC neurons. Here we report a novel transgenic mouse expressing human wild-type asyn under control of the noradrenergic-specific dopamine β-hydroxylase promoter. These mice developed oligomeric and conformation-specific asyn in LC neurons, alterations in hippocampal and LC microglial abundance, upregulated GFAP expression, degeneration of LC fibers, decreased striatal dopamine (DA) metabolism, and age-dependent behaviors reminiscent of non-motor symptoms of PD that were rescued by adrenergic receptor antagonists. These mice provide novel insights into how asyn pathology affects LC neurons and how central noradrenergic dysfunction may contribute to early PD pathophysiology.

Significance statement

α-synuclein (asyn) pathology and loss of neurons in the locus coeruleus (LC) are two of the most ubiquitous neuropathologic features of Parkinson's disease (PD). Dysregulated NE neurotransmission is associated with the non-motor symptoms of PD including sleep disturbances, emotional changes such as anxiety and depression, and cognitive decline. Importantly, loss of central NE may contribute to the chronic inflammation in, and progression of, PD. We have generated a novel transgenic mouse expressing human asyn in LC neurons to investigate how increased asyn expression affects the function of the central noradrenergic transmission and associated behaviors. We report cytotoxic effects of oligomeric and conformation-specific asyn, astrogliosis, LC fiber degeneration, disruptions in striatal dopamine metabolism, and age-dependent alterations in non-motor behaviors without inclusions.

Introduction

Brain regions affected in Parkinson's disease (PD) exhibit proteinaceous aggregates (known as Lewy bodies) primarily composed of α-synuclein (asyn), chronic inflammation, and neuron loss (den Hartog and Bethlem, 1960; Spillantini et al., 1997; Tansey and Goldberg, 2010). In addition to deficiencies in striatal dopamine (DA) and the DA transporter (DAT), acetylcholine, serotonin, and norepinephrine (NE) systems are also affected (Gonera et al., 1997; Abbott et al., 2005; Ross et al., 2008).

The locus coeruleus (LC) is among the first brain regions affected in PD. The LC is a bilateral pontine nucleus at the lateral floor of the fourth ventricle, and is the main source of NE for the central nervous system (CNS) (Iversen et al., 1983; Mann et al., 1983; Braak et al., 2001). Asyn aggregates and neuronal degeneration in the LC are ubiquitous features of PD and are associated with non-motor symptoms including sleep disorders,

96 mood disturbances, and cognitive deficits (Iversen et al., 1983; Chui et al., 1986; German
97 et al., 1992; Braak et al., 2001; Zarow et al., 2003; Weinshenker, 2018). Imaging and
98 histological studies show a progressive loss of central NE, noradrenergic neurons, and
99 accumulation of asyn pathology in the LC in PD (Halliday et al., 1990; German et al.,
100 1992; Brunnstrom et al., 2011; Pifl et al., 2012; Keren et al., 2015) which may exacerbate
101 degeneration of DA neurons in the midbrain substantia nigra pars compacta (SNpc)
102 (Zarow et al., 2003; Chen et al., 2014).
103 Depleting LC-NE exacerbates 6-hydroxydopamine (6-OHDA) or 1-methyl-4phenyl-
104 1,2,3,6-tetrahydropyridine (MPTP)-induced nigrostriatal pathology in rodents and
105 primates (Mavridis et al., 1991; Srinivasan and Schmidt, 2003; Rommelfanger et al.,
106 2007), while increasing extracellular NE is protective (Kilbourn et al., 1998;
107 Rommelfanger et al., 2004; Kreiner et al., 2019). Furthermore, lesioning LC neurons
108 induces inflammation, and dysregulated NE neurotransmission may contribute to the
109 chronic inflammation seen in PD (Kim and Joh, 2006; Tansey and Goldberg, 2010; Yao
110 et al., 2015; Bharani et al., 2017; Song et al., 2018).
111 The initiating event in asyn aggregation in sporadic PD is unclear, but candidate
112 mechanisms include increased expression of asyn, as individuals with a multiplication
113 mutation in the gene encoding asyn (*SNCA*) develop autosomal dominantly-inherited PD
114 (Singleton et al., 2003; Chartier-Harlin et al., 2004; Ferese et al., 2015). Age is the primary
115 risk factor for PD, and rodent models of asyn overexpression develop age-dependent
116 asyn aggregates and PD-like behavioral abnormalities (Masliah et al., 2000; Giasson et
117 al., 2002; Hansen et al., 2013). However, in most of these models, transgene expression
118 is driven by a pan-neuronal promoter with asyn overexpression in multiple regions of the

119 CNS, with only one model reporting LC pathology (Masliah et al., 2000; Giasson et al.,
120 2002; Maskri et al., 2004; Schell et al., 2009; Koprich et al., 2010; Sotiriou et al., 2010;
121 Delenclos et al., 2017). Viral-mediated expression has been used to target asyn
122 overexpression to specific brain regions (Baekelandt et al., 2002; Kirik et al., 2002;
123 Delenclos et al., 2017; Ip et al., 2017; Niu et al., 2018). Notably, viral overexpression of a
124 familial PD mutant asyn in LC neurons resulted in asyn aggregation, inflammation, and
125 degeneration of LC neurons (Henrich et al., 2018).
126 To investigate specifically how pathology induced by increases in asyn affects
127 noradrenergic neurons in the LC in an aging organism, we targeted expression of human
128 wild-type asyn to LC neurons under control of the noradrenergic/adrenergic-specific
129 dopamine β-hydroxylase (DBH) promoter using bacterial artificial chromosome (BAC)
130 transgenesis. To determine the molecular, cellular, and behavioral age-dependent
131 consequences of increased asyn expression in LC neurons, 3-, 14-, and 24-month (mo)
132 old DBH-hSNCA transgenic (Tg) mice and non-transgenic (nTg) littermate controls were
133 examined.

134 **Methods**

135 **Experimental design.** To determine how expression of human asyn in LC neurons
136 affects neuronal health and LC-NE-associated behaviors, mice were aged undisturbed
137 until the time of behavioral testing or sacrifice at ages 3-, 14-, and 24-mos.

138 **Generation of the DBH-hSNCA mouse model.** Male and female mice expressing
139 human wild-type α-synuclein (DBH-hSNCA) were engineered using a commercially
140 available human bacterial artificial chromosomal (BAC) RP11-746P3 (Cubells et al.,
141 2016) encompassing the *DBH* gene. The wild-type *hSNCA* cDNA open reading frame

142 (400bp) was targeted to the translational start site of *DBH* by standard BAC
143 recombineering methods by the University of North Carolina – Chapel Hill Molecular
144 Neuroscience Core (currently Animal Model Core). The BAC construct was injected into
145 C57BL/6N pronuclei by the Emory University Mouse Transgenic and Gene Targeting
146 Core Facility (http://www.cores.emory.edu/tmc/index.html), transgene expression in
147 founder pups was determined by PCR, and breeding lines were established. Mice
148 carrying the hSNCA sequence were crossed with wild-type C57Bl/6N mice (Charles
149 River) to establish the hemizygous transgenic DBH-hSNCA line.
150 To improve efficiency and accuracy of LC tissue isolation for western blot and mRNA
151 analysis, DBH-hSNCA mice were crossed with the TH-EGFP reporter mouse expressing
152 enhanced green fluorescent protein (EGFP) under the tyrosine hydroxylase (TH)
153 promotor (Sawamoto et al., 2001).
154 **Animals.** Male and female DBH-hSNCA mice were maintained on a C57Bl/6 background.
155 Mice were group housed (maximum 5 mice per cage) until two weeks prior to the start of
156 behavioral testing, when they were singly housed until euthanized. Animals were
157 maintained on a 12/12h light/dark cycle with access to standard rodent chow and water
158 *ad libitum*. Hemizygous animals served as experimental mice, with non-transgenic
159 littermates as controls. Genotypes were determined by tail snip PCR with two sets of
160 primers: Forward 5' TGTCCAAGATGGACCAGACTC 3' Reverse 3'
161 ACTGGTCTGAGGCAGGGAGCA 5'; Set Forward 5' GCCCTCAGTCTACTTGCGGGA 3'
162 Reverse 3' GCGAGAGCATCATAGGGAGT 5'. Experimental procedures involving use of
163 animals were performed in accordance with the NIH Guidelines for Animal Care and Use

164 and approved by the Institutional Animal Care and Use Committee at Emory University
165 School of Medicine.

166 **Sleep latency test.** Latency to fall asleep was quantified as the duration of time following
167 gentle handling until their first sleep bout, which was defined as sleeping continuously for
168 2 min, and for a total of 75% of the 10-min period that began at sleep onset (Hunsley and
169 Palmiter, 2004). Sleep testing began at 9 AM, 2 h into the light cycle when internal
170 pressure to sleep is high. The sessions were video recorded and scored by
171 an experienced observer blind to the genotype. We have validated this behavioral sleep
172 scoring method with EEG (Porter-Stransky et al., 2019).

173 **Marble burying test.** Marble burying was conducted as previously described (de Sousa
174 Rodrigues et al., 2017) to determine whether expression of human asyn in LC neurons
175 promotes anxiety-like behavior. Mice were placed in a plastic tub (50.5 x 39.4 x 19.7 cm)
176 containing 5 inches of lightly pressed bedding. Twenty marbles of uniform size and color
177 were placed in 5 rows of 4 marbles each on top of the bedding. Mice were placed in the
178 containers and allowed to roam freely for 30 min. At the end of testing, the mice were
179 placed back into home cages, and the number of marbles buried at least two-thirds of
180 their height were counted. Marble burying was conducted 2 weeks after sleep latency
181 testing.

182 **Open Field testing.** In the open field test, a mouse that spends less time in or hesitates
183 to re-enter the open center of the testing chamber is considered to be exhibiting anxiety-
184 like behavior (Britton and Britton, 1981). During the light phase of the light/dark cycle,
185 mice were acclimated to a dark testing room under red light for 1 h before testing. Mice
186 were placed into the open field (45 cm X 45 cm square box) and allowed to move freely

for 10 min. Distance, velocity, center, and border statistics were measured using Noldus/Ethovision software. Center was defined as the central 22.5 cm X 22.5 cm. Open field was conducted 1 week after marble burying.

Circadian locomotion. All testing mice were acclimated to the testing room for 2 d prior to the experiment. Mice were each placed in a clear Plexiglas (15.75” L, 13.25” L, 7.38” H) activity cage equipped with infrared photobeams (San Diego Instruments, La Jolla, CA). Food and water were available *ad libitum* during the 23-h testing period. Ambulations (consecutive photobeam breaks) were recorded by PAS software. Circadian locomotion behavior was assessed 2 weeks after open field testing.

Fear conditioning. Fear conditioning training and contextual and cued fear testing is a test of memory for the association of an aversive stimulus with an environment cue or context, and was conducted as previously described (Chalermpalanupap et al., 2018) over 3 consecutive days. Mice were placed in the fear conditioning apparatus (7” W, 7” D, 12” H, Coulbourn) with metal shock grid floor and allowed to explore the enclosure for 3 min. Following habituation, three conditioned stimulus (CS)-unconditioned stimulus (US) pairings were presented with a one-min inter-trial interval. The CS was a 20 sec 85 db tone, and the US was a 2 sec 0.5mA footshock (Precision Animal Shocker, Colbourn) which co-terminated with CS presentation. The contextual test was conducted on the following day when animals were placed back into the same chamber. On day three, the animals were placed in a novel compartment and allowed to habituate for 2 min. Following habituation, the 85 db tone was presented, and the amount of freezing behavior recorded. No shocks were given during the contextual or cued tests. Fear conditioning was conducted 1 week after circadian locomotion behavior.

210 **Behavioral pharmacology.** For the three days prior to pharmacological experiments,
211 mice received vehicle administration to habituate them to intraperitoneal (i.p.) injections.
212 On the day of testing, mice received vehicle or a cocktail of the α1-adrenergic receptor
213 antagonist prazosin (0.5 mg/kg; Sigma-Adrich, St. Louis, MO) and the β-adrenergic
214 receptor antagonist DL-propranolol (5 mg/kg; Sigma-Aldrich), immediately prior to sleep
215 latency testing. Drug doses were chosen based on previous studies and optimized in pilot
216 experiments to ensure that behavioral effects were not due to sedation (Vazey and Aston-
217 Jones, 2014). Treatments were counterbalanced between subjects, all mice received
218 vehicle or drug cocktail with a seven-day washout period between testing days.
219 **Tissue collection.** Animals used in immunohistochemical and high-performance liquid
220 chromatography (HPLC) analyses were anesthetized by injection of sodium pentobarbital
221 (Euthasol, Virbac) until unresponsive. Mice were transcardially perfused with phosphate-
222 buffered saline (PBS; pH 7.4) until exiting blood ran clear. Brain tissue was removed, with
223 one hemisphere post-fixed in 4% paraformaldehyde for immunohistochemistry, and the
224 other dissected and flash frozen for HPLC. Animals used for qPCR or western blot
225 analyses were euthanized by cervical dislocation under isoflurane anesthesia. Tissue was
226 flash frozen and stored at -80°C until processing.
227 **Immunofluorescence and analysis.** Brain tissue was sectioned on a freezing
228 microtome (Leica SM2010R, Buffalo Grove, IL) at 40 μm and stored in cryoprotectant
229 (30% ethylene glycol, 30% sucrose, 13.32 mM NaH_2PO_4, 38.74 mM Na_2HPO_4, 250 μM
230 Polyvinylpyrrolidone) solution at -20°C until staining. Sections were washed in PBS before
231 blocking in 5% normal goat serum (Jackson ImmunoResearch 005-000-121; NGS) with
232 0.05% Triton X-100 (Sigma #T9284100) in Tris-buffered saline pH 7.4 (TBS) for 1 h at

233 room temperature. Sections were transferred directly to primary antibody solution
234 containing 1% NGS, 0.05% Triton-X 100, and antibody at the concentrations described
235 in Table 1 and incubated overnight at room temperature (05-02 Ms anti-NET) or 4°C (all
236 other primary antibodies). Fluorescently conjugated secondary antibodies (described in
237 Table 1) were diluted in 0.1% NGS with 0.05% Triton X-100, and tissue sections were
238 incubated for 1 h at room temperature in the dark. Sections were mounted on Superfrost
239 Plus slides (VWR) and were coverslipped with Vectashield with DAPI (Vector). All
240 immunofluorescent images were acquired as z-stack images and the file compressed on
241 a Keyence BZ-X700 microscope system (Itasca, IL). The Allen Brain Atlas version 1
242 (2008) was used to identify regions of interest (ROIs). One section per mouse containing
243 the dorsal hippocampus (near bregma -1.995 mm) and one containing the LC (bregma -
244 5.555 mm) were analyzed for percent immunoreactivity (IR) within a standard ROI. A
245 detection threshold was set uniformly across images in each analysis, and % IR
246 determined using the "Measure" feature of ImageJ. Percent IR was calculated as area of
247 IR within the ROI divided by the total ROI area and multiplied by 100. Quantification of
248 Iba1-positive cells (microglia) was also analyzed with a standard threshold, ROI, and
249 upper and lower size limits (pixel^2) using the "Analyze particles" function in ImageJ.
250 **Immunohistochemistry and analysis.** For immunoperoxidase visualization of pSer129
251 asyn (Rutherford et al., 2016) and conformation-specific asyn, brains were post-fixed with
252 4% paraformaldehyde, incubated in 70% ethanol, and then embedded in paraffin. Paraffin
253 sections were cut at 5μm and stained using previously published protocols (Joers et al.,
254 2014; Lloyd et al., 2020). Briefly, sections were deparaffinized and rehydrated, and heat-
255 induced antigen retrieval was performed using 10mM sodium citrate solution (pH 6.0,

256 pSer129) or citrate Target Retrieval Solution (Dako #S169984-2, pH 6.1) with 0.05%
257 Tween-20 (conformation-specific) for 30 min. Next, endogenous peroxidase was blocked,
258 and non-specific binding sites minimized with 8% serum (Jackson ImmunoResearch),
259 20% avidin/biotin blocking solution (Vector Laboratories #SP-2001), and 0.1% Triton-X
260 100 in TBS for 1 h (pser129) or with 2% FBS in 0.1M Tris (pH 7.6) for 10 min
261 (conformation-specific). Sections were transferred into primary antibody solution
262 containing 5% serum, and 20% avidin/biotin blocking solution (Vector Laboratories #SP-
263 2001) in TBS (pSer129) or 2% FBS in 0.1M Tris (conformation-specific) and antibody
264 concentrations detailed in Table 1 overnight at 4°C. The sections were then incubated in
265 appropriate biotinylated secondary antibodies diluted with 5% serum in TBS (pser129) for
266 30 min or 2% FBS in 0.1M Tris for 1 h (conformation-specific) at room temperature.
267 Antigen signal was amplified using VectaStain ABC-HRP Elite kit (Vector Laboratories
268 #PK-6100) for 1 h at room temperature, and staining was developed using 3,3-
269 diaminobenzine (DAB) as the chromogen (Sigma, #D4293). Sections were
270 counterstained with Mayer's hematoxylin (Sigma #51275). Sections stained for
271 conformation-specific asyn underwent additional blocking with 2% FBS in 0.1M Tris
272 before secondary antibody and DAB incubations. All DAB-immunostained slides were
273 imaged with a Leica microscope (DMi8 Thunder) and post-processed through Adobe
274 Photoshop to improve contrast. Intensity of conformation-specific asyn-IR in the LC were
275 scored by experimenters blinded to genotype using the following rubric: 0 = no staining
276 in the LC; 1 = < 25% of the LC stained; 2 = 25-50% of the LC stained; 3 = > 50% of the
277 LC stained. Images for pser129 asyn were not quantified.

278 **Proximity ligation assay (PLA).** Paraffin-embedded tissue was rehydrated by
279 consecutive incubations in xylene, Histoclear, 100% ethanol, 95% ethanol, 70% ethanol
280 and H_2O. Samples were then incubated in 10% H_2O_2 in PBS to reduce background and
281 heated in a microwave in citrate buffer (pH 6.0; Abcam) for antigen retrieval. After antigen
282 retrieval, samples were processed for immunofluorescence: 1 h RT incubation in 10%
283 serum with 0.05% Tween-20 in TBS block, 1 h incubation in primary antibody, and TBS
284 with 0.05% Tween-20 (TBS-T) wash. Slides were then incubated for 1 h with secondary
285 antibodies conjugated to Alexa488 (Life Technologies) and washed again with TBS-T.
286 For immunohistochemistry, samples were then coverslipped with FluorSave
287 (Calbiochem). For PLA, samples were covered in manufacturers PLA blocking solution
288 (Sigma) for 1 h at 37°C, and then incubated overnight with PLA conjugates (a-syn211;
289 ab80627 Abcam). The next day, samples were washed with TBS-T, incubated in ligation
290 solution for 1 h at 37° C, washed with TBS-T, incubated in amplification solution for 2.5 h
291 at 37°C, washed with TBS, counterstained with DAPI, and mounted with FluorSave. All
292 PLA reagents were used per manufacturer's instructions (Sigma #92008). PLA puncta
293 were counted by experimenters blinded to genotype from 25 cells per LC section per
294 animal. Two independent experimental rounds were normalized and averaged to provide
295 the final quantification.
296 **Dot blots**. Frozen LC samples were homogenized in RIPA buffer (1% Triton-X 100,
297 50mM Tris HCL, 0.1% sodium dodecyl sulfate, 150mM NaCL, pH 8.0), or Trizol (Life
298 Technologies #15596-018) and centrifuged at 12,000 x g for 10 min. Supernatants were
299 transferred to fresh tubes and quantified for protein concentration by BCA assay.
300 Samples were diluted in PBS, and 225 ng was spotted directly onto nitrocellulose

301 membranes (Biorad #1620117) for dot blot analysis (Sampson et al., 2016). Membranes
302 were air-dried for 10 min and blocked in TBS-T containing 5% non-fat dry milk for 1 h.
303 Membranes were probed for conformation-specific asyn (Table 1) at 4°C overnight with
304 gentle rocking. Membranes were incubated with HRP-conjugated secondary antibodies,
305 followed by SuperSignal™ West Pico PLUS Chemiluminescent Substrate
306 (ThermoScientific) and imaged using a Licor (Odyssey FC) system.
307 **RNA Scope.** *In situ* RNA analysis was performed using RNAScope Multiplex Fluorescent
308 v2 kit (ACD Bio 3231000). Tissue prep and analysis were conducted as described in
309 manufacturer's protocol. Briefly, following transcardial perfusion with saline, brains were
310 incubated in 4% paraformaldehyde (PFA) for 24 hours followed by a series of increasing
311 sucrose concentrations before being frozen in optimal temperature cutting medium
312 (Sakura) and stored at -80°C until sectioning. Tissue sections (12μm) were collected on
313 a Leica CM1900 cryostat and mounted on Superfrost Plus slides. To prevent tissue
314 detachment, slides were dried at 60°C for 30 min and fixed in 4% PFA for 15 min at 4°C
315 before ethanol dehydration. Tissue was processed as described in ACD Bio protocol
316 (acdbio.com/technical-support/user-manuals #323100-USM).
317 **Western immunoblotting.** Western blots were conducted as previously described (de
318 Sousa Rodrigues et al., 2017). Flash frozen samples were stored at -80°C until
319 processing. Protein was isolated from LC samples with RIPA buffer. RIPA samples were
320 centrifuged at 12,000 rpm for 20 min at 4°C. Supernatant was transferred to new tube for
321 bicinchoninic acid protein assay (Pierce Scientific #23225). Trizol samples were
322 resuspended in 1% SDS. Samples were diluted to 1μg/μl in 4x sample buffer (BioRad
323 #1610747) and boiled at 90°C for 5 min. Electrophoresis was performed using 12% gels

324 (BioRad #4568046; 5µl) and transferred to 0.45 µm PVDF membrane using Trans-Blot
325 Turbo Transfer System (BioRad). For immunoblotting, the membrane was fixed in 0.4%
326 PFA for 30 min following transfer. After a brief wash, blots were incubated in 5% milk
327 blocking buffer (BioRad) for 1 hour at 4°C before primary antibody overnight at 4°C (See
328 Table 1). Membranes were washed with TBS-T (0.01% Tween-20) and incubated in HRP-
329 conjugated secondary antibodies in blocking buffer for 1 hour at room temperature.
330 Images were acquired using Azure Biosystems and analyzed by ImageStudio Lite
331 software. Protein expression was normalized to total protein (Li-Cor #926-11015).

332 **High performance liquid chromatography (HPLC).**

333 Monoamines were examined by high performance liquid chromatography with
334 electrochemical detection as described previously (Song et al., 2012). For HPLC, an ESA
335 5600A CoulArray detection system, equipped with an ESA Model 584 pump and an ESA
336 542 refrigerated autosampler was used. Separations were performed using an MD-150 ×
337 3.2 mm C18 (3 µM) column at 25ºC. The mobile phase consisted of 8% acetonitrile, 75
338 mM NaH_2PO4, 1.7 mM 1-octanesulfonic acid sodium and 0.025% trimethylamine at pH
339 2.9. Twenty-five microliters of sample were injected. The samples were eluted
340 isocratically at 0.4 mL/min and detected using a 6210-electrochemical cell (ESA, Bedford,
341 MA) equipped with 5020 guard cell. Guard cell potential was set at 475 mV, while
342 analytical cell potentials were −175, 150, 350 and 425 mV. The analytes were identified
343 by the matching criteria of retention time and sensor ratio measures to known standards
344 (Sigma Chemical Co., St. Louis MO.) consisting of dopamine, norepinephrine, 3,4-
345 dihydroxyphenylacetic acid (DOPAC), and 4-Hydroxy-3-methoxyphenylglycol (MHPG).

346 Compounds were quantified by comparing peak areas to those of standards on the
347 dominant sensor.

348 **Statistical analysis.** Student's t-test was used to assess differences by genotype within
349 each age group in sleep latency, marble burying, open field, western blot, and all
350 immunofluorescent analyses. Repeated measures two-way ANOVA was used to analyze
351 differences by genotype (between-subject) for within-subject conditions including fear
352 conditioning and circadian locomotor assay followed by Tukey's post hoc test where
353 applicable. Analyses were conducted within each age group. Comparisons across age
354 groups were not conducted, as behavioral assays, HPLC, and immunofluorescence of
355 each cohort were conducted at separate time points. The analyses were performed using
356 GraphPad Prism 7 (GraphPad Software, Inc., La Jolla, CA) with a p-value threshold of
357 <0.05.

358 **Results**

359 **Generation of DBH-hSNCA mice**

360 The DBH-hSNCA mouse model was developed using a DBH-BAC construct carrying the
361 wild type human *SNCA* cDNA open reading frame at the translational start site of *DBH*
362 (Fig. 1). Transgene integration was confirmed by PCR, and founder mice were bred with
363 wild type C57BL/6 mice to establish the hemizygous DBH-hSNCA line.

364 **Human *Snca* mRNA is expressed in DBH-hSNCA LC neurons**

365 Fluorescent *in situ* mRNA analysis revealed human *Snca* mRNA in Tg LC neurons (Fig.
366 2), which co-localized with mouse *Th* and mouse *Dbh* mRNA, while human *Snca* mRNA
367 expression was not detected in nTg LC neurons.

368 **Human asyn is expressed in select noradrenergic brainstem nuclei of DBH-hSNCA**
369 **transgenic mice**
370 Human asyn protein in the LC was analyzed by immunofluorescence and western blot.
371 Using an antibody specific for human asyn (Biolegend 807801), expression of human
372 asyn was found to co-localize with TH-expressing LC neurons only in brain sections from
373 DBH-hSNCA Tg mice (Fig. 3A). No human asyn-specific immunofluorescence was
374 detected in LC neurons of nTg littermates or in SNpc neurons regardless of genotype
375 (Fig. 3A,C). Human asyn was also detectable specifically in LC protein lysate from Tg
376 tissue by immunoblot and not in nTg lysates (Fig. 3B; n=4). Quantitative western blot
377 analysis of LC protein using a pan-asyn antibody to detect both human and mouse asyn
378 protein revealed a significant ~30% increase of total asyn in Tg mice at 3-mo relative to
379 that in nTg littermates (Fig. 3D; $t_{(6)}$=3.156, p=0.0197, n=4). Human *SNCA* mRNA
380 expression in Tg LC neurons was confirmed by qPCR (Data not shown). Expression of
381 human asyn was confirmed in the A4 (Fig. 3G) and A5 (Fig. 3H) DBH-expressing regions
382 in the pons of Tg mice by immunofluorescence, but expression was not detectable in the
383 medullary A1/C1 (Fig. 3E) or A2/C2 (Fig. 3F) nuclei of DBH-hSNCA mice.
384 **DBH-hSNCA mice exhibit behavioral phenotypes that resemble features of non-**
385 **motor PD symptoms**
386 A primary role of the LC-NE system is promoting arousal and wakefulness; LC activity is
387 highest just prior to, and during wake (Hobson et al., 1975). Sleep disturbances are one
388 of the most common non-motor PD symptoms, and PD patients with disturbed sleep have
389 greater asyn pathology in the LC than PD patients without sleep complaints (Kalaitzakis
390 et al., 2013). Thus, sleep latency was assessed to examine whether features of the

391 sleep/wake cycle were affected by human asyn expression in the LC. Mice were gently
392 handled and returned to their home cage, and video recording was scored by an observer
393 blind to the genotype to determine latency to fall asleep. Our findings indicate that there
394 was a significant increase in sleep latency in Tg mice at 3-mos, (Fig. 4A; $t_{(14)}$=4.36
395 p=0.0007; n=8) and 14-mos ($t_{(17)}$=2.51, p=0.0225; n= 9 nTg & 10 Tg), indicative of an
396 elevated arousal state. No differences were observed at 24-mos ($t_{(8)}$=0.821, p=0.4354,
397 n= 8 nTg & 7 Tg).
398 Central noradrenergic neurons, including the LC and A2 regions, are activated by stress
399 exposure, and blocking LC activity abolishes stress-induced anxiety-like behavior
400 (Rinaman, 2011; McCall et al., 2015). In PD, anxiety severity is inversely correlated with
401 LC function (Remy et al., 2005). To examine anxiety-like behavior, the behavior DBH-
402 hSNCA mice was assessed in marble burying and open field tests. In the marble burying
403 assay, there was a significant increase in the number of marbles buried by Tg mice at 14-
404 (Fig. 4B; $t_{(18)}$=2.735, p=0.0136; n= 8 nTg & 12 Tg) and 24-mos ($t_{(13)}$=2.212, p=0.0455, n=
405 8 nTg & 7 Tg) but not at 3-mos ($t_{(13)}$=1.369, p=0.1942, n= 7 nTg & 8 Tg). In open field
406 tests, an age-dependent anxiety-like phenotype was also evident in 14-mo Tg mice,
407 evinced by an increase in the latency to re-enter the center of the testing field (Fig. 4C;
408 $t_{(17)}$2.359, p=0.0305; n= 7 nTg & 12 Tg), with no differences in 3- ($t_{(11)}$=0.1988, p=0.8460,
409 n= 8 nTg & 5 Tg) or 24-mo old animals ($t_{(11)}$=0.5075, p=0.6219, n= 5 nTg & 5 Tg). The
410 latency to enter the center score for one 24-mo nTg animal was omitted after failing to
411 enter the center during the open field test.
412 Fear conditioning is a measure of hippocampal-dependent (contextual) or -independent
413 (cued) associative learning (Phillips and LeDoux, 1992), and mice lacking NE exhibit

414 impaired contextual learning (Murchison et al., 2004). In a standard fear conditioning
415 paradigm, 14-mo old DBH-hSNCA Tg mice exhibited increased freezing behavior during
416 the fear training session (Fig. 4D center; Interaction $F_{(6, 120)}$=2.735, p=0.0159; n=8-14), as
417 well as during the contextual test (Fig. 4E center; effect of genotype $F_{(1, 20)}$=5.566,
418 p=0.0286), with no differences in freezing behavior during the cued test (Fig. 4F;
419 Interaction $F_{(7, 160)}$=0.5146, p=0.8128). No genotype differences were found at 3- or 24-
420 months in the fear training (Fig. 4D; 3-mos Interaction $F_{(6,72)}$= 1.082, p=0.3815, n=7; 24-
421 mos Interaction $F_{(6, 78)}$=0.3783, p=0.8908, n = 8 nTg & 7 Tg), contextual test (Fig. 4E; 3-
422 mos Interaction $F_{(7, 84)}$= 0.1477, n=7; p=0.9938; 24-mos Interaction $F_{(7, 91)}$=1.040,
423 p=0.4089, n = 8 nTg & 7 Tg) or cued test (Fig. 4F; 3-mos Interaction $F_{(8, 96)}$=1.508,
424 p=0.1645, n=7; 24-mos Interaction $F_{(8, 104)}$=0.2766, p=0.9723, n = 8 nTg & 7 Tg) .
425 Because disruption in locomotor activity can affect behavioral testing, we evaluated the
426 locomotion over 24 h and found no genotype differences at 3-mos (Interaction $F_{(21,}$
427 $_{252)}$=1.033, p=0.4233; n=7), 14-mos (Interaction $F_{(21, 231)}$=0.6319, p=0.8929; n= 7 nTg & 6
428 Tg), or 24-mos ($F_{(21, 273)}$=0.06975, p=0.8349; n= 8 nTg & 7 Tg) of age (Fig. 4F). Initially,
429 all groups had high levels of activity, as would be expected in a novel environment, which
430 decreased as mice habituated to the test apparatus. Ambulations increased normally in
431 all genotypes at commencement of the dark phase, when mice are typically more active,
432 and decreased once the next light cycle began.

433 **Sleep latency in 3-, and 14-mo old DBH-hSNCA mice is normalized by adrenergic**
434 **receptor blockade**

435 The behavioral results above (i.e. increased arousal and anxiety-like behavior) were
436 consistent with overactive LC-NE transmission. To test this hypothesis, an additional

437 cohort of 3- and 14-mo old DBH-hSNCA mice underwent sleep latency testing following
438 administration of saline or a cocktail of propranolol (β-adrenergic receptor antagonist) and
439 prazosin (α1-adrenergic receptor antagonist). Similar to baseline testing, 3- and 14-mo
440 Tg mice administered saline took longer to fall asleep than nTg littermates. However,
441 adrenergic receptor blockade normalized sleep latency in 3-mo old or 14-mo old Tg mice,
442 while propranolol and prazosin administration had no effect on sleep latency in nTg mice
443 (Fig. 5A; Interaction $F_{(1,\ 16)}$=7.367, p=0.0153, n=5) (Fig. 5B; Interaction $F_{(1,\ 18)}$=1.27,
444 p=0.0035, n= 6 nTg & 5 Tg).

445 **Human asyn forms oligomers and conformation-specific asyn in LC neurons at 14-**
446 **and 24-mos of age**

447 To determine whether transgenic expression of human asyn in LC neurons resulted in
448 formation of asyn oligomers, tissue sections containing the LC were analyzed using a
449 human asyn proximity ligation assay (PLA). Tg LC neurons displayed more asyn puncta
450 per TH-positive neuron than nTg LC neurons at 14 ($t_{(8)}$=2.53, p=0.0352; n=4 nTg & 6 Tg)
451 and 24 months of age ($t_{(8)}$=2.402, p=0.0430; n=12 nTg & 3 Tg) (Fig. 6A,B). To investigate
452 whether the oligomeric asyn had altered conformation, we probed LC tissue lysates from
453 3-month old Tg and nTg mice for immunoreactivity against an asyn filament conformation-
454 specific antibody (MJFR14) and tyrosine hydroxylase (TH) on immune-dot blots, using
455 Snca knock-out and M83 asyn transgenic mouse tissues as negative and positive
456 controls, respectively. We found that only Tg mice displayed robust MJFR14-IR (Fig. 6C),
457 and it trended to be negatively correlated to TH in the LC (Fig. 6D), suggesting increased
458 asyn may downregulate TH expression and/or induce dysfunction. We next probed for
459 conformation-specific asyn properties using an immunohistological approach and found

460 significant variability in the intensity of MJFR14-IR in LC neuron sections of 24-month old
461 Tg and nTg mice that did not reach statistical significance between genotypes (Fig. 6E,F).
462 Lastly, because conformation-specific and aggregated asyn has been associated with
463 increased phosphorylation at serine 129 (pSer129), and labeling these forms of the
464 protein is commonly used to identify asyn inclusions (Fujiwara et al., 2002; Wakamatsu
465 et al., 2007; Schell et al., 2009), we immunolabeled LC tissue sections with antibodies
466 specific for fibril-rich asyn (Syn-F1, data not shown) and asyn pSer129 (EP1536Y and
467 LS4-2G12; Fig. 6G) and found no differences between genotypes, suggesting that at 24-
468 mos of age there are no mature higher-order asyn inclusions in DBH-hSNCA mice.

469 **Human asyn expression in LC neurons impacts striatal dopamine metabolism in**
470 **24-mo old mice**

471 Dysregulated catecholamine metabolism and degeneration of catecholaminergic neurons
472 are well-established features of PD (Iversen et al., 1983; Mann et al., 1983; Hirsch et al.,
473 1988; Fearnley and Lees, 1991). Therefore, we measured catecholamine levels using
474 high-performance liquid chromatography (HPLC). Hippocampal and striatal tissue
475 content of NE, the NE metabolite MHPG, DA, and the DA metabolite DOPAC were
476 quantified, revealing that NE (Fig. 7A,B) and DA (Fig. 7E,F) were not significantly affected
477 in the hippocampus or striatum at any age. Similarly, the ratio of the major NE metabolite
478 MHPG to NE was unaffected (Fig. 7C,D). The ratio of the DA metabolite DOPAC to DA
479 in the hippocampus was unaltered (Fig. 7G), but was significantly reduced in the Tg
480 striatum at 24-mos (Fig. 7H; $t_{(10)}$=3.546, p=0.0046; n= 9 nTg & 6 Tg), consistent with
481 decreased DA turnover.

482 **Human asyn expression does not affect LC neuronal integrity**

483 LC neurons were visualized using NET-IR. NET is a reliable marker of LC neurons, and
484 its expression is reduced in PD patients (Remy et al., 2005). Using a standard ROI, no
485 difference in the percent NET IR was detected between genotypes at 3- (Fig. 8;
486 $t_{(17)}$=0.4537, p=0.6558; n= 9 nTg & 10 Tg), 14- ($t_{(10)}$=0.8908, p=0.3939; n= 7 nTg & 5 Tg),
487 or 24-mos ($t_{(8)}$=0.8069, p=0.4430; n=5).

488 **Elevation of tyrosine hydroxylase in the LC of DBH-hSNCA mice**

489 Tyrosine hydroxylase (TH) is the rate-limiting enzyme in NE and DA synthesis, and its
490 long-term activity depends on its expression levels (Levitt et al., 1965; Haycock, 1993;
491 Kumer and Vrana, 1996). To determine whether TH expression in the LC is affected by
492 human asyn, we assessed TH IR in sections from 3-, 14-, and 24-mo old mice. TH IR was
493 normalized to NET IR to control for potential differences in Bregma level between
494 sections. TH expression was increased in Tg LC neurons (Fig. 9A,B) at both 3-
495 ($t_{(17)}$=2.154, p=0.0459; n= 9 nTg & 10 Tg) and 14-mo ($t_{(10)}$=2.463, p=0.0335; n= 7 nTg &
496 5 Tg) of age. Western blot analysis from 3-mo old TH-EGFP-expressing LC neurons (Fig.
497 9C,D) confirmed higher TH expression in Tg animals ($t_{(10)}$=3.837, p=0.0033; n= 6 nTg &
498 5 Tg).

499 **Human asyn expression in LC neurons affects expression of local inflammatory**
500 **markers**

501 A wealth of studies suggest that dysregulated noradrenergic neurotransmission is
502 associated with inflammation (reviewed by Butkovich et al., 2018), and that dysregulation
503 of the LC-NE system could contribute to the chronic neuroinflammation observed in PD
504 (Fujita et al., 1998; Gyoneva and Traynelis, 2013; Johnson et al., 2013). To determine
505 whether human asyn expression in LC neurons affects the number of myeloid cells in the

506 brain (both brain-resident microglia and potentially infiltrating monocytes), we quantified
507 the number of Iba1-positive cells in the LC by immunofluorescence. At 14-mo, there was
508 a significant decrease in the number of Iba1-expressing cells in the LC of Tg animals (Fig.
509 10A,B; $t_{(13)}$=2.845, p=0.0138; n=7), with no changes at other ages. To determine
510 astrocyte activation, we quantified glial fibrillary acidic protein (GFAP) IR, commonly used
511 as a protein marker of astrogliosis (Eng and Ghirnikar, 1994), in the LC. At 24-mo, there
512 was a significant increase in astrocytic GFAP expression in the LC of Tg animals (Fig.
513 10C, D; $t_{(10)}$=2.744, p=0.0207; n= 7 nTg & 4 Tg).

514 **Hippocampal astrogliosis and changes in number of hippocampal Iba1-expressing**
515 **cells in DBH-hSNCA mice**

516 To determine whether degeneration of hippocampal LC projections is associated with
517 inflammation, GFAP IR was visualized in the CA1, CA3, and dentate gyrus regions of the
518 hippocampus. At 14-mos, there was a significant increase in GFAP expression in CA1
519 (Fig. 11A,B; $t_{(19)}$=2.723 ,p=0.0135, n= 12 nTg & 9 Tg) and CA3 (Fig. 11E,F; $t_{(19)}$=2.275
520 ,p=0.0347, n = 12 nTg & 9 Tg) but not the dentate gyrus (Fig. 11C,D; $t_{(19)}$=1.607,
521 p=0.1246, n= 12 nTg & 12 Tg) of Tg mice compared to nTg. Similar to what we observed
522 in the LC, the number of Iba1-expressing cells in CA1 was reduced in Tg mice at 14-mos
523 (Fig. 12; $t_{(16)}$=2.592, p=0.0196, n=9).

524 **Human asyn expression in LC neurons is associated with loss of hippocampal LC**
525 **fibers at 24-mos**

526 The LC is the sole source of hippocampal NE, which is necessary for proper memory
527 formation and retrieval (Devauges and Sara, 1991). Noradrenergic LC fibers express
528 NET, and PD brain tissue shows substantial LC denervation (Pavese et al., 2011). To

529 determine whether hippocampal LC projections degenerate in DBH-hSNCA mice, we
530 examined NET IR in the CA1, CA3, and dentate gyrus regions of the hippocampus. At
531 24-mos, we found a reduction in LC fibers in the dentate gyrus (Fig. 13C,D; $t_{(10)}$=2.974,
532 p=0.0156; n= 6 nTg & 5 Tg), with a trend for reduction in CA1 (Fig. 13A, B; $t_{(10)}$=1.899,
533 p=0.0901, n= 6 nTg & 5 Tg) and CA3 (Fig. 13E,F; $t_{(10)}$=1.538, p=0.1585, n= 6 nTg & 5
534 Tg). No differences were observed in mice at 3-, or 14-mos.

535 **Discussion**

536 Based on a wealth of evidence (Mavridis et al., 1991; Srinivasan and Schmidt, 2003; Tong
537 et al., 2006; Rommelfanger et al., 2007; Yao et al., 2015), we posit that asyn pathology
538 and degeneration of LC neurons may represent a tipping point in PD progression;
539 therefore, understanding how asyn accumulation in LC neurons affects their function and
540 survival may help inform development of new therapeutics for earlier interventions. To
541 this end, we developed a new BAC transgenic mouse expressing human wild-type asyn
542 under the control of the noradrenergic-specific DBH.

543 Human asyn was detectable by immunofluorescence in the Tg LC and in neurons of some
544 (e.g. A4, A5) but not other (e.g. A1, A2) additional DBH-expressing brainstem nuclei by
545 immunofluorescence at 3-mos. Analysis of total asyn (mouse + human) by western blot
546 revealed that the total asyn burden is increased in Tg LC neurons at 3-mos. While
547 pSer129-positive and fibrillar pathological inclusions were not detected in LC neurons at
548 24-mos, increasing the burden of asyn expression in LC neurons resulted in the formation
549 of putative asyn oligomers, as detected by PLA. We did find nonuniform biochemical and
550 immunohistolocigal evidence of conformation-specific asyn-IR (MJFR14) in 3- and 24-
551 month old Tg mice, suggesting a change in the structural conformation of asyn in some

552 animals, possibly as a consequence of human asyn burden, the corruption of endogenous
553 asyn, or another critical intrinsic, animal-specific factor such as altered TH, which a trend
554 was found to be negatively correlated to the level of conformation-specific asyn by dot
555 blot in 3-month old Tg mice. Although we observed no loss of LC cell bodies, NET-
556 expressing fibers were reduced in the hippocampus of 24-mo old mice. This finding
557 resembles the pattern of neuron death observed in PD, with axon terminals degenerating
558 prior to frank cell loss in the LC (Hornykiewicz, 1998). Interestingly, the selective loss of
559 LC fibers in the dentate gyrus of DBH-hSNCA mice is reminiscent of what we observed
560 in TgF344-AD rat model of Alzheimer's disease that accumulates tau pathology in the LC
561 (Rorabaugh et al., 2017). To determine the functional outcome of human asyn expression
562 in LC neurons, we measured catecholamine levels in the hippocampus and striatum.
563 Despite the loss of hippocampal LC fibers at 24-mos, we did not detect changes in
564 hippocampal NE content by HPLC, which may indicate a compensatory enhancement in
565 NE synthesis. We observed a trend toward decreased striatal NE 24-mos, but it was not
566 statistically significant. With the sparse noradrenergic innervation to the striatum, it is
567 possible that changes in NE neurotransmission are detectable there prior to more densely
568 innervated regions. Dysregulated DA metabolism is a central feature of PD (Leenders et
569 al., 1990), and midbrain dopaminergic innervation to the striatum is modulated by LC-NE
570 (Lategan et al., 1990; Grenhoff et al., 1993; Rommelfanger et al., 2007; Rommelfanger
571 and Weinshenker, 2007). Studies of catecholamine function in rodents show that
572 enhancing LC-NE stimulates midbrain DA release in the striatum, whereas LC lesions or
573 NE deficiency reduce striatal DA release (Lategan et al., 1990; Grenhoff et al., 1993;
574 Schank et al., 2006). We found that at 24-mos, Tg mice had a reduced striatal ratio of

575 DOPAC:DA and a trend toward increased DA, suggesting that human asyn expression in
576 aging LC neurons causes a reduction in striatal DA turnover. Future studies will determine
577 whether NE innervation to midbrain DA neurons is reduced in 24-mo DBH-hSNCA mice,
578 and whether loss of noradrenergic transmission impairs striatal DA release. While no
579 significant differences were detected in hippocampal or striatal NE content at any age, Tg
580 LC neurons had increased TH expression at 3- and 14-mos relative to nTg littermates,
581 suggesting an increased capacity for NE synthesis.
582 Neuroinflammation is a central feature of PD pathology (McGeer et al., 1988; Gerhard et
583 al., 2006; Tansey and Goldberg, 2010), with extensive evidence of changes in microglial
584 activation in brain regions that degenerate in PD (Kim and Joh, 2006; Tansey and
585 Goldberg, 2010), and we know that microglia and astrocyte functions are modulated by
586 NE neurotransmission (Fahrig, 1993; Heneka et al., 2010; Bharani et al., 2017).
587 Unexpectedly, we observed fewer Iba1-expressing cells in the LC and CA1 region of the
588 hippocampus of DBH-hSNCA mice at 14-mos compared to nTg littermates. It has been
589 reported that NE can modulate microglial activity, and the functional outcome of microglia
590 adrenergic receptor activation appears to depend on the physiological context (Fujita et
591 al., 1998; Gyoneva and Traynelis, 2013; Johnson et al., 2013). At 14-mos, there was an
592 increase in hippocampal astrocytic GFAP expression. Astrocytes throughout the brain are
593 activated by NE, and AR signaling stimulates calcium transients and promotes the release
594 of inflammatory signaling molecules by astrocytes (Norris and Benveniste, 1993; Duffy
595 and MacVicar, 1995; Paukert et al., 2014). However, the number of GFAP-expressing
596 astrocytes is inversely correlated to the amount of dopaminergic cell loss in PD, and
597 increased GFAP-IR in the hippocampus occurred prior to loss of LC projections (Damier

598 et al., 1993; Eng and Ghirnikar, 1994). Further studies are required to determine whether
599 increased GFAP activity is due to dysregulated NE neurotransmission, or an inflammatory
600 response secondary to degeneration of LC projections.
601 Historically, the LC has been implicated in arousal state and stress responses. For
602 example, LC activity tracks with sleep cycles (with highest firing during wake and
603 immediately preceding sleep-wake transitions), and chemogenetic or optogenetic
604 activation of LC neurons increases wakefulness (Carter et al., 2010; Vazey and Aston-
605 Jones, 2014; Porter-Stransky et al., 2019). Furthermore, the LC is activated by stress,
606 and stimulation of LC neurons elicits anxiety-like behaviors (Valentino and Van
607 Bockstaele, 2008; McCall et al., 2015). DBH-hSNCA mice exhibited age-dependent
608 behavioral phenotypes that peaked at 14-mos and are consistent with LC hyperactivity
609 and increased NE transmission. Specifically, compared to nTg littermates, DBH-hSNCA
610 mice displayed increased arousal (as measured by latency to fall asleep), anxiety-like
611 behavior (as measured by marble burying and latency to re-enter the center of an open
612 field), and stress responses (as measured by freezing during fear conditioning training
613 and context re-exposure). These phenotypes are relevant to multiple non-motor
614 symptoms of PD. Sleep disturbances are one of the most common complaints of PD
615 patients, and patients who experience disturbed sleep appear to have greater LC asyn
616 pathology than those who do not report sleep disturbances (Kalaitzakis et al., 2013).
617 Anxiety is also a common complaint, as up to 60% of PD patients report experiencing
618 anxiety (Chaudhuri and Schapira, 2009; Lin et al., 2015). Importantly, DBH-hSNCA mice
619 did not display changes in the number or speed of ambulations relative to nTg mice at
620 any age examined, ruling out a general locomotor abnormality that has been observed in

621 more ubiquitous asyn overexpression mice (Giasson et al., 2002; Fleming et al., 2004;
622 Graham and Sidhu, 2010). Reducing DA specifically in DA-neurons causes motor, but
623 not most non-motor, deficits in mice, which further indicates that these symptoms arise
624 from alterations in distinct neurotransmitter systems (Jiang et al., 2020). In fact, the
625 increased sleep latency observed in Tg animals was normalized by blocking α1- and β-
626 adrenergic receptors, which suggests that the behavioral phenotype is due to enhanced
627 noradrenergic neurotransmission. We have previously speculated that asyn pathology
628 promotes LC hyperactivity and non-motor symptoms during PD progression prior to the
629 degeneration of noradrenergic neurons later in the disease (Weinshenker, 2018), and the
630 present data support that idea. Indeed, the behavioral phenotypes we observed were
631 most prominent at 14-mos, while degeneration of LC fibers was not evident until 24-mos,
632 a time when behavioral abnormalities abated. There are several potential mechanisms
633 by which increases in human asyn may be affecting the LC-NE system (Fig. 14). TH
634 protein was increased in 3- and 14-mo old Tg mice, which is when behavioral phenotypes
635 consistent with NE over-activity emerged. Because TH is the rate-limiting enzyme in NE
636 production, this may reflect increased NE synthetic capacity, although the relevance is
637 not clear because we did not detect differences in tissue NE content. Human wild-type
638 asyn has been reported to increase in the size, and delay in the closing, of the vesicular
639 fusion pore, allowing more neurotransmitter to spill into the extracellular space (Larsen et
640 al., 2006; Logan et al., 2017). In addition, viral-mediated overexpression of A53T mutant
641 asyn in LC neurons causes increased firing rate (Henrich et al., 2018). Alternatively, if
642 human asyn expression is negatively impacting LC neuron health as suggested by the
643 presence of asyn oligomers and the loss of hippocampal LC fibers at 24-mos, there may

644 be compensatory increases in neuronal activity. Chemical lesion of LC neurons
645 transiently increases NE neurotransmission by increasing neuronal firing frequency and
646 activity patterns (Szot et al., 2016). Future studies directly examining LC neuron firing and
647 NE release will be necessary to identify the mechanism in play here.
648 LC neurons are among the first affected in PD, and the features of DBH-hSNCA mice
649 may represent early pathology and non-motor components of PD that provide insight into
650 the functional impact of human asyn expression in LC neurons during aging. Importantly,
651 our data suggest that overexpression of wild-type human asyn and formation of oligomers
652 alone is sufficient for the LC dysfunction, fiber degeneration, and behavioral deficits we
653 observed, while asyn pSer129 inclusions are not required for these phenotypes.
654 Additionally, studies involving exposure to environmental factors that synergize with asyn
655 expression to influence the risk of PD will likely elucidate the genetic and environmental
656 interactions that contribute to LC involvement in the pre-clinical pre-motor stages of PD,
657 as well as the impact of LC degeneration on the trajectory of PD pathogenesis.
658

659 **References**

660

661 Abbott RD, Ross GW, White LR, Tanner CM, Masaki KH, Nelson JS, Curb JD, Petrovitch H (2005)
662 Excessive daytime sleepiness and subsequent development of Parkinson disease.
663 Neurology 65:1442-1446.
664 Baekelandt V, Claeys A, Eggermont K, Lauwers E, De Strooper B, Nuttin B, Debyser Z (2002)
665 Characterization of lentiviral vector-mediated gene transfer in adult mouse brain. Hum
666 Gene Ther 13:841-853.
667 Bharani KL, Derex R, Granholm AC, Ledreux A (2017) A noradrenergic lesion aggravates the
668 effects of systemic inflammation on the hippocampus of aged rats. PLoS One
669 12:e0189821.
670 Braak E, Sandmann-Keil D, Rub U, Gai WP, de Vos RA, Steur EN, Arai K, Braak H (2001) alpha-
671 synuclein immunopositive Parkinson's disease-related inclusion bodies in lower brain
672 stem nuclei. Acta Neuropathol 101:195-201.
673 Britton DR, Britton KT (1981) A sensitive open field measure of anxiolytic drug activity.
674 Pharmacol Biochem Behav 15:577-582.
675 Brunnstrom H, Friberg N, Lindberg E, Englund E (2011) Differential degeneration of the locus
676 coeruleus in dementia subtypes. Clin Neuropathol 30:104-110.
677 Butkovich LM, Houser MC, Tansey MG (2018) alpha-Synuclein and Noradrenergic Modulation of
678 Immune Cells in Parkinson's Disease Pathogenesis. Front Neurosci 12:626.
679 Carter ME, Yizhar O, Chikahisa S, Nguyen H, Adamantidis A, Nishino S, Deisseroth K, de Lecea L
680 (2010) Tuning arousal with optogenetic modulation of locus coeruleus neurons. Nat
681 Neurosci 13:1526-1533.
682 Chalermpalanupap T, Schroeder JP, Rorabaugh JM, Liles LC, Lah JJ, Levey AI, Weinshenker D
683 (2018) Locus Coeruleus Ablation Exacerbates Cognitive Deficits, Neuropathology, and
684 Lethality in P301S Tau Transgenic Mice. J Neurosci 38:74-92.
685 Chartier-Harlin MC, Kachergus J, Roumier C, Mouroux V, Douay X, Lincoln S, Levecque C, Larvor
686 L, Andrieux J, Hulihan M, Waucquier N, Defebvre L, Amouyel P, Farrer M, Destee A
687 (2004) Alpha-synuclein locus duplication as a cause of familial Parkinson's disease.
688 Lancet 364:1167-1169.
689 Chaudhuri KR, Schapira AH (2009) Non-motor symptoms of Parkinson's disease: dopaminergic
690 pathophysiology and treatment. Lancet Neurol 8:464-474.
691 Chen X, Huddleston DE, Langley J, Ahn S, Barnum CJ, Factor SA, Levey AI, Hu X (2014)
692 Simultaneous imaging of locus coeruleus and substantia nigra with a quantitative
693 neuromelanin MRI approach. Magn Reson Imaging 32:1301-1306.
694 Chui HC, Mortimer JA, Slager U, Zarow C, Bondareff W, Webster DD (1986) Pathologic
695 correlates of dementia in Parkinson's disease. Arch Neurol 43:991-995.
696 Cubells JF, Schroeder JP, Barrie ES, Manvich DF, Sadee W, Berg T, Mercer K, Stowe TA, Liles LC,
697 Squires KE, Mezher A, Curtin P, Perdomo DL, Szot P, Weinshenker D (2016) Human
698 Bacterial Artificial Chromosome (BAC) Transgenesis Fully Rescues Noradrenergic
699 Function in Dopamine beta-Hydroxylase Knockout Mice. PLoS One 11:e0154864.
700 Damier P, Hirsch EC, Zhang P, Agid Y, Javoy-Agid F (1993) Glutathione peroxidase, glial cells and
701 Parkinson's disease. Neuroscience 52:1-6.

de Sousa Rodrigues ME, Bekhbat M, Houser MC, Chang J, Walker DI, Jones DP, Oller do Nascimento CMP, Barnum CJ, Tansey MG (2017) Chronic psychological stress and high-fat high-fructose diet disrupt metabolic and inflammatory gene networks in the brain, liver, and gut and promote behavioral deficits in mice. Brain Behav Immun 59:158-172.

Delenclos M, Faroqi AH, Yue M, Kurti A, Castanedes-Casey M, Rousseau L, Phillips V, Dickson DW, Fryer JD, McLean PJ (2017) Neonatal AAV delivery of alpha-synuclein induces pathology in the adult mouse brain. Acta Neuropathol Commun 5:51.

den Hartog JW, Bethlem J (1960) The distribution of Lewy bodies in the central and autonomic nervous systems in idiopathic paralysis agitans. J Neurol Neurosurg Psychiatry 23:283-290.

Devauges V, Sara SJ (1991) Memory retrieval enhancement by locus coeruleus stimulation: evidence for mediation by beta-receptors. Behav Brain Res 43:93-97.

Duffy S, MacVicar BA (1995) Adrenergic calcium signaling in astrocyte networks within the hippocampal slice. J Neurosci 15:5535-5550.

Eng LF, Ghirnikar RS (1994) GFAP and astrogliosis. Brain Pathol 4:229-237.

Fahrig T (1993) Receptor subtype involved and mechanism of norepinephrine-induced stimulation of glutamate uptake into primary cultures of rat brain astrocytes. Glia 7:212-218.

Fearnley JM, Lees AJ (1991) Ageing and Parkinson's disease: substantia nigra regional selectivity. Brain 114 (Pt 5):2283-2301.

Ferese R, Modugno N, Campopiano R, Santilli M, Zampatti S, Giardina E, Nardone A, Postorivo D, Fornai F, Novelli G, Romoli E, Ruggieri S, Gambardella S (2015) Four Copies of SNCA Responsible for Autosomal Dominant Parkinson's Disease in Two Italian Siblings. Parkinsons Dis 2015:546462.

Fleming SM, Salcedo J, Fernagut PO, Rockenstein E, Masliah E, Levine MS, Chesselet MF (2004) Early and progressive sensorimotor anomalies in mice overexpressing wild-type human alpha-synuclein. J Neurosci 24:9434-9440.

Fujita H, Tanaka J, Maeda N, Sakanaka M (1998) Adrenergic agonists suppress the proliferation of microglia through beta 2-adrenergic receptor. Neurosci Lett 242:37-40.

Fujiwara H, Hasegawa M, Dohmae N, Kawashima A, Masliah E, Goldberg MS, Shen J, Takio K, Iwatsubo T (2002) alpha-Synuclein is phosphorylated in synucleinopathy lesions. Nat Cell Biol 4:160-164.

Gerhard A, Pavese N, Hotton G, Turkheimer F, Es M, Hammers A, Eggert K, Oertel W, Banati RB, Brooks DJ (2006) In vivo imaging of microglial activation with [11C](R)-PK11195 PET in idiopathic Parkinson's disease. Neurobiol Dis 21:404-412.

German DC, Manaye KF, White CL, 3rd, Woodward DJ, McIntire DD, Smith WK, Kalaria RN, Mann DM (1992) Disease-specific patterns of locus coeruleus cell loss. Ann Neurol 32:667-676.

Giasson BI, Duda JE, Quinn SM, Zhang B, Trojanowski JQ, Lee VM (2002) Neuronal alpha-synucleinopathy with severe movement disorder in mice expressing A53T human alpha-synuclein. Neuron 34:521-533.

Gonera EG, van't Hof M, Berger HJ, van Weel C, Horstink MW (1997) Symptoms and duration of the prodromal phase in Parkinson's disease. Mov Disord 12:871-876.

745 Graham DR, Sidhu A (2010) Mice expressing the A53T mutant form of human alpha-synuclein
746 exhibit hyperactivity and reduced anxiety-like behavior. J Neurosci Res 88:1777-1783.
747 Grenhoff J, Nisell M, Ferre S, Aston-Jones G, Svensson TH (1993) Noradrenergic modulation of
748 midbrain dopamine cell firing elicited by stimulation of the locus coeruleus in the rat. J
749 Neural Transm Gen Sect 93:11-25.
750 Gyoneva S, Traynelis SF (2013) Norepinephrine modulates the motility of resting and activated
751 microglia via different adrenergic receptors. J Biol Chem 288:15291-15302.
752 Halliday GM, Li YW, Blumbergs PC, Joh TH, Cotton RG, Howe PR, Blessing WW, Geffen LB (1990)
753 Neuropathology of immunohistochemically identified brainstem neurons in Parkinson's
754 disease. Ann Neurol 27:373-385.
755 Hansen C, Bjorklund T, Petit GH, Lundblad M, Murmu RP, Brundin P, Li JY (2013) A novel alpha-
756 synuclein-GFP mouse model displays progressive motor impairment, olfactory
757 dysfunction and accumulation of alpha-synuclein-GFP. Neurobiol Dis 56:145-155.
758 Haycock JW (1993) Multiple signaling pathways in bovine chromaffin cells regulate tyrosine
759 hydroxylase phosphorylation at Ser19, Ser31, and Ser40. Neurochem Res 18:15-26.
760 Heneka MT, Nadrigny F, Regen T, Martinez-Hernandez A, Dumitrescu-Ozimek L, Terwel D,
761 Jardanhazi-Kurutz D, Walter J, Kirchhoff F, Hanisch UK, Kummer MP (2010) Locus
762 ceruleus controls Alzheimer's disease pathology by modulating microglial functions
763 through norepinephrine. Proc Natl Acad Sci U S A 107:6058-6063.
764 Henrich MT, Geibl FF, Lee B, Chiu WH, Koprich JB, Brotchie JM, Timmermann L, Decher N,
765 Matschke LA, Oertel WH (2018) A53T-alpha-synuclein overexpression in murine locus
766 coeruleus induces Parkinson's disease-like pathology in neurons and glia. Acta
767 Neuropathol Commun 6:39.
768 Hirsch E, Graybiel AM, Agid YA (1988) Melanized dopaminergic neurons are differentially
769 susceptible to degeneration in Parkinson's disease. Nature 334:345-348.
770 Hobson JA, McCarley RW, Wyzinski PW (1975) Sleep cycle oscillation: reciprocal discharge by
771 two brainstem neuronal groups. Science 189:55-58.
772 Hornykiewicz O (1998) Biochemical aspects of Parkinson's disease. Neurology 51:S2-9.
773 Hunsley MS, Palmiter RD (2004) Altered sleep latency and arousal regulation in mice lacking
774 norepinephrine. Pharmacol Biochem Behav 78:765-773.
775 Ip CW, Klaus LC, Karikari AA, Visanji NP, Brotchie JM, Lang AE, Volkmann J, Koprich JB (2017)
776 AAV1/2-induced overexpression of A53T-alpha-synuclein in the substantia nigra results
777 in degeneration of the nigrostriatal system with Lewy-like pathology and motor
778 impairment: a new mouse model for Parkinson's disease. Acta Neuropathol Commun
779 5:11.
780 Iversen LL, Rossor MN, Reynolds GP, Hills R, Roth M, Mountjoy CQ, Foote SL, Morrison JH,
781 Bloom FE (1983) Loss of pigmented dopamine-beta-hydroxylase positive cells from locus
782 coeruleus in senile dementia of Alzheimer's type. Neurosci Lett 39:95-100.
783 Jiang S, Berger S, Hu Y, Bartsch D, Tian Y (2020) Alterations of the Motor and Olfactory
784 Functions Related to Parkinson's Disease in Transgenic Mice With a VMAT2-Deficiency in
785 Dopaminergic Neurons. Front Neurosci 14:356.
786 Joers V, Dilley K, Rahman S, Jones C, Shultz J, Simmons H, Emborg ME (2014) Cardiac
787 sympathetic denervation in 6-OHDA-treated nonhuman primates. PLoS One 9:e104850.

788 Johnson JD, Zimomra ZR, Stewart LT (2013) Beta-adrenergic receptor activation primes
789 microglia cytokine production. J Neuroimmunol 254:161-164.
790 Kalaitzakis ME, Gentleman SM, Pearce RK (2013) Disturbed sleep in Parkinson's disease:
791 anatomical and pathological correlates. Neuropathol Appl Neurobiol 39:644-653.
792 Keren NI, Taheri S, Vazey EM, Morgan PS, Granholm AC, Aston-Jones GS, Eckert MA (2015)
793 Histologic validation of locus coeruleus MRI contrast in post-mortem tissue. Neuroimage
794 113:235-245.
795 Kilbourn MR, Sherman P, Abbott LC (1998) Reduced MPTP neurotoxicity in striatum of the
796 mutant mouse tottering. Synapse 30:205-210.
797 Kim YS, Joh TH (2006) Microglia, major player in the brain inflammation: their roles in the
798 pathogenesis of Parkinson's disease. Exp Mol Med 38:333-347.
799 Kirik D, Rosenblad C, Burger C, Lundberg C, Johansen TE, Muzyczka N, Mandel RJ, Bjorklund A
800 (2002) Parkinson-like neurodegeneration induced by targeted overexpression of alpha-
801 synuclein in the nigrostriatal system. J Neurosci 22:2780-2791.
802 Koprich JB, Johnston TH, Reyes MG, Sun X, Brotchie JM (2010) Expression of human A53T alpha-
803 synuclein in the rat substantia nigra using a novel AAV1/2 vector produces a rapidly
804 evolving pathology with protein aggregation, dystrophic neurite architecture and
805 nigrostriatal degeneration with potential to model the pathology of Parkinson's disease.
806 Mol Neurodegener 5:43.
807 Kreiner G, Rafa-Zablocka K, Barut J, Chmielarz P, Kot M, Baginska M, Parlato R, Daniel WA,
808 Nalepa I (2019) Stimulation of noradrenergic transmission by reboxetine is beneficial for
809 a mouse model of progressive parkinsonism. Sci Rep 9:5262.
810 Kumer SC, Vrana KE (1996) Intricate regulation of tyrosine hydroxylase activity and gene
811 expression. J Neurochem 67:443-462.
812 Larsen KE, Schmitz Y, Troyer MD, Mosharov E, Dietrich P, Quazi AZ, Savalle M, Nemani V,
813 Chaudhry FA, Edwards RH, Stefanis L, Sulzer D (2006) Alpha-synuclein overexpression in
814 PC12 and chromaffin cells impairs catecholamine release by interfering with a late step
815 in exocytosis. J Neurosci 26:11915-11922.
816 Lategan AJ, Marien MR, Colpaert FC (1990) Effects of locus coeruleus lesions on the release of
817 endogenous dopamine in the rat nucleus accumbens and caudate nucleus as
818 determined by intracerebral microdialysis. Brain Res 523:134-138.
819 Leenders KL, Salmon EP, Tyrrell P, Perani D, Brooks DJ, Sager H, Jones T, Marsden CD,
820 Frackowiak RS (1990) The nigrostriatal dopaminergic system assessed in vivo by positron
821 emission tomography in healthy volunteer subjects and patients with Parkinson's
822 disease. Arch Neurol 47:1290-1298.
823 Levitt M, Spector S, Sjoerdsma A, Udenfriend S (1965) Elucidation of the Rate-Limiting Step in
824 Norepinephrine Biosynthesis in the Perfused Guinea-Pig Heart. J Pharmacol Exp Ther
825 148:1-8.
826 Lin CH, Lin JW, Liu YC, Chang CH, Wu RM (2015) Risk of Parkinson's disease following anxiety
827 disorders: a nationwide population-based cohort study. Eur J Neurol 22:1280-1287.
828 Lloyd GM, Trejo-Lopez JA, Xia Y, McFarland KN, Lincoln SJ, Ertekin-Taner N, Giasson BI, Yachnis
829 AT, Prokop S (2020) Prominent amyloid plaque pathology and cerebral amyloid
830 angiopathy in APP V717I (London) carrier - phenotypic variability in autosomal dominant
831 Alzheimer's disease. Acta Neuropathol Commun 8:31.

832 Logan T, Bendor J, Toupin C, Thorn K, Edwards RH (2017) alpha-Synuclein promotes dilation of
833 the exocytotic fusion pore. Nat Neurosci 20:681-689.
834 Mann JJ, Stanley M, Kaplan RD, Sweeney J, Neophytides A (1983) Central catecholamine
835 metabolism in vivo and the cognitive and motor deficits in Parkinson's disease. J Neurol
836 Neurosurg Psychiatry 46:905-910.
837 Maskri L, Zhu X, Fritzen S, Kuhn K, Ullmer C, Engels P, Andriske M, Stichel CC, Lubbert H (2004)
838 Influence of different promoters on the expression pattern of mutated human alpha-
839 synuclein in transgenic mice. Neurodegener Dis 1:255-265.
840 Masliah E, Rockenstein E, Veinbergs I, Mallory M, Hashimoto M, Takeda A, Sagara Y, Sisk A,
841 Mucke L (2000) Dopaminergic loss and inclusion body formation in alpha-synuclein
842 mice: implications for neurodegenerative disorders. Science 287:1265-1269.
843 Mavridis M, Degryse AD, Lategan AJ, Marien MR, Colpaert FC (1991) Effects of locus coeruleus
844 lesions on parkinsonian signs, striatal dopamine and substantia nigra cell loss after 1-
845 methyl-4-phenyl-1,2,3,6-tetrahydropyridine in monkeys: a possible role for the locus
846 coeruleus in the progression of Parkinson's disease. Neuroscience 41:507-523.
847 McCall JG, Al-Hasani R, Siuda ER, Hong DY, Norris AJ, Ford CP, Bruchas MR (2015) CRH
848 Engagement of the Locus Coeruleus Noradrenergic System Mediates Stress-Induced
849 Anxiety. Neuron 87:605-620.
850 McGeer PL, Itagaki S, Boyes BE, McGeer EG (1988) Reactive microglia are positive for HLA-DR in
851 the substantia nigra of Parkinson's and Alzheimer's disease brains. Neurology 38:1285-
852 1291.
853 Murchison CF, Zhang XY, Zhang WP, Ouyang M, Lee A, Thomas SA (2004) A distinct role for
854 norepinephrine in memory retrieval. Cell 117:131-143.
855 Niu H, Shen L, Li T, Ren C, Ding S, Wang L, Zhang Z, Liu X, Zhang Q, Geng D, Wu X, Li H (2018)
856 Alpha-synuclein overexpression in the olfactory bulb initiates prodromal symptoms and
857 pathology of Parkinson's disease. Transl Neurodegener 7:25.
858 Norris JG, Benveniste EN (1993) Interleukin-6 production by astrocytes: induction by the
859 neurotransmitter norepinephrine. J Neuroimmunol 45:137-145.
860 Paukert M, Agarwal A, Cha J, Doze VA, Kang JU, Bergles DE (2014) Norepinephrine controls
861 astroglial responsiveness to local circuit activity. Neuron 82:1263-1270.
862 Pavese N, Rivero-Bosch M, Lewis SJ, Whone AL, Brooks DJ (2011) Progression of monoaminergic
863 dysfunction in Parkinson's disease: a longitudinal 18F-dopa PET study. Neuroimage
864 56:1463-1468.
865 Phillips RG, LeDoux JE (1992) Differential contribution of amygdala and hippocampus to cued
866 and contextual fear conditioning. Behav Neurosci 106:274-285.
867 Pifl C, Kish SJ, Hornykiewicz O (2012) Thalamic noradrenaline in Parkinson's disease: deficits
868 suggest role in motor and non-motor symptoms. Mov Disord 27:1618-1624.
869 Porter-Stransky KA, Centanni SW, Karne SL, Odil LM, Fekir S, Wong JC, Jerome C, Mitchell HA,
870 Escayg A, Pedersen NP, Winder DG, Mitrano DA, Weinshenker D (2019) Noradrenergic
871 Transmission at Alpha1-Adrenergic Receptors in the Ventral Periaqueductal Gray
872 Modulates Arousal. Biol Psychiatry 85:237-247.
873 Remy P, Doder M, Lees A, Turjanski N, Brooks D (2005) Depression in Parkinson's disease: loss
874 of dopamine and noradrenaline innervation in the limbic system. Brain 128:1314-1322.

875 Rinaman L (2011) Hindbrain noradrenergic A2 neurons: diverse roles in autonomic, endocrine,
876 cognitive, and behavioral functions. Am J Physiol Regul Integr Comp Physiol 300:R222-
877 235.
878 Rommelfanger KS, Weinshenker D (2007) Norepinephrine: The redheaded stepchild of
879 Parkinson's disease. Biochem Pharmacol 74:177-190.
880 Rommelfanger KS, Weinshenker D, Miller GW (2004) Reduced MPTP toxicity in noradrenaline
881 transporter knockout mice. J Neurochem 91:1116-1124.
882 Rommelfanger KS, Edwards GL, Freeman KG, Liles LC, Miller GW, Weinshenker D (2007)
883 Norepinephrine loss produces more profound motor deficits than MPTP treatment in
884 mice. Proc Natl Acad Sci U S A 104:13804-13809.
885 Rorabaugh JM, Chalermpalanupap T, Botz-Zapp CA, Fu VM, Lembeck NA, Cohen RM,
886 Weinshenker D (2017) Chemogenetic locus coeruleus activation restores reversal
887 learning in a rat model of Alzheimer's disease. Brain 140:3023-3038.
888 Ross GW, Petrovitch H, Abbott RD, Tanner CM, Popper J, Masaki K, Launer L, White LR (2008)
889 Association of olfactory dysfunction with risk for future Parkinson's disease. Ann Neurol
890 63:167-173.
891 Rutherford NJ, Brooks M, Giasson BI (2016) Novel antibodies to phosphorylated alpha-synuclein
892 serine 129 and NFL serine 473 demonstrate the close molecular homology of these
893 epitopes. Acta Neuropathol Commun 4:80.
894 Sampson TR, Debelius JW, Thron T, Janssen S, Shastri GG, Ilhan ZE, Challis C, Schretter CE, Rocha
895 S, Gradinaru V, Chesselet MF, Keshavarzian A, Shannon KM, Krajmalnik-Brown R,
896 Wittung-Stafshede P, Knight R, Mazmanian SK (2016) Gut Microbiota Regulate Motor
897 Deficits and Neuroinflammation in a Model of Parkinson's Disease. Cell 167:1469-1480
898 e1412.
899 Sawamoto K, Nakao N, Kobayashi K, Matsushita N, Takahashi H, Kakishita K, Yamamoto A,
900 Yoshizaki T, Terashima T, Murakami F, Itakura T, Okano H (2001) Visualization, direct
901 isolation, and transplantation of midbrain dopaminergic neurons. Proc Natl Acad Sci U S
902 A 98:6423-6428.
903 Schank JR, Ventura R, Puglisi-Allegra S, Alcaro A, Cole CD, Liles LC, Seeman P, Weinshenker D
904 (2006) Dopamine beta-hydroxylase knockout mice have alterations in dopamine
905 signaling and are hypersensitive to cocaine. Neuropsychopharmacology 31:2221-2230.
906 Schell H, Hasegawa T, Neumann M, Kahle PJ (2009) Nuclear and neuritic distribution of serine-
907 129 phosphorylated alpha-synuclein in transgenic mice. Neuroscience 160:796-804.
908 Singleton AB et al. (2003) alpha-Synuclein locus triplication causes Parkinson's disease. Science
909 302:841.
910 Song CH, Fan X, Exeter CJ, Hess EJ, Jinnah HA (2012) Functional analysis of dopaminergic
911 systems in a DYT1 knock-in mouse model of dystonia. Neurobiol Dis 48:66-78.
912 Song S, Jiang L, Oyarzabal EA, Wilson B, Li Z, Shih YI, Wang Q, Hong JS (2018) Loss of Brain
913 Norepinephrine Elicits Neuroinflammation-Mediated Oxidative Injury and Selective
914 Caudo-Rostral Neurodegeneration. Mol Neurobiol.
915 Sotiriou E, Vassilatis DK, Vila M, Stefanis L (2010) Selective noradrenergic vulnerability in alpha-
916 synuclein transgenic mice. Neurobiol Aging 31:2103-2114.
917 Spillantini MG, Schmidt ML, Lee VM, Trojanowski JQ, Jakes R, Goedert M (1997) Alpha-synuclein
918 in Lewy bodies. Nature 388:839-840.

919 Srinivasan J, Schmidt WJ (2003) Potentiation of parkinsonian symptoms by depletion of locus
920 coeruleus noradrenaline in 6-hydroxydopamine-induced partial degeneration of
921 substantia nigra in rats. Eur J Neurosci 17:2586-2592.
922 Szot P, Franklin A, Miguelez C, Wang Y, Vidaurrazaga I, Ugedo L, Sikkema C, Wilkinson CW,
923 Raskind MA (2016) Depressive-like behavior observed with a minimal loss of locus
924 coeruleus (LC) neurons following administration of 6-hydroxydopamine is associated
925 with electrophysiological changes and reversed with precursors of norepinephrine.
926 Neuropharmacology 101:76-86.
927 Tansey MG, Goldberg MS (2010) Neuroinflammation in Parkinson's disease: its role in neuronal
928 death and implications for therapeutic intervention. Neurobiol Dis 37:510-518.
929 Tong J, Hornykiewicz O, Kish SJ (2006) Inverse relationship between brain noradrenaline level
930 and dopamine loss in Parkinson disease: a possible neuroprotective role for
931 noradrenaline. Arch Neurol 63:1724-1728.
932 Valentino RJ, Van Bockstaele E (2008) Convergent regulation of locus coeruleus activity as an
933 adaptive response to stress. Eur J Pharmacol 583:194-203.
934 Vazey EM, Aston-Jones G (2014) Designer receptor manipulations reveal a role of the locus
935 coeruleus noradrenergic system in isoflurane general anesthesia. Proc Natl Acad Sci U S
936 A 111:3859-3864.
937 Wakamatsu M, Ishii A, Ukai Y, Sakagami J, Iwata S, Ono M, Matsumoto K, Nakamura A, Tada N,
938 Kobayashi K, Iwatsubo T, Yoshimoto M (2007) Accumulation of phosphorylated alpha-
939 synuclein in dopaminergic neurons of transgenic mice that express human alpha-
940 synuclein. J Neurosci Res 85:1819-1825.
941 Weinshenker D (2018) Long Road to Ruin: Noradrenergic Dysfunction in Neurodegenerative
942 Disease. Trends Neurosci 41:211-223.
943 Yao N, Wu Y, Zhou Y, Ju L, Liu Y, Ju R, Duan D, Xu Q (2015) Lesion of the locus coeruleus
944 aggravates dopaminergic neuron degeneration by modulating microglial function in
945 mouse models of Parkinsons disease. Brain Res 1625:255-274.
946 Zarow C, Lyness SA, Mortimer JA, Chui HC (2003) Neuronal loss is greater in the locus coeruleus
947 than nucleus basalis and substantia nigra in Alzheimer and Parkinson diseases. Arch
948 Neurol 60:337-341.
949
950

951 **Figure Legends**
952
953 **Figure 1:** *hSNCA* cDNA open reading frame was targeted to the translational start site of
954 *DBH* by standard BAC recombineering methods
955
956 **Figure 2: Human *Snca* mRNA is expressed in DBH-hSNCA locus coeruleus**
957 **neurons.** Human *Snca* mRNA (hSnca; white) expression is detectable only in transgenic
958 (Tg: bottom row) LC neurons, where it co-localizes with mouse *Th* mRNA (mTh, green),
959 and mouse *Dbh* mRNA (mDbh; red) using RNA Scope Fluorescent Multiplex v2 assay.
960 Scale bar = 50μm.
961
962 **Figure 3: Analysis of asyn expression in catecholaminergic brainstem regions of**
963 **young DBH-hSNCA mice. *A,*** Immunofluorescent detection of human asyn (red) with a
964 species-specific antibody (Biolegend 807801) demonstrates co-localization with TH-
965 expressing LC neurons (green) in Tg mice (lower panel) but not in nTg mice (upper
966 panel), or in ***C,*** TH-expressing neurons (green) in the substantia nigra regardless of
967 genotype. ***B,*** Human asyn protein is expressed selectively in LC neurons of Tg mice by
968 western blot. ***D,*** Immunoblot of LC protein with an antibody against asyn that detects the
969 mouse and human protein reveals a significant increase in total asyn protein expression
970 in Tg LC neurons as compared to that in LC of nTg littermate mice. Immunoblot data
971 graphed as arbitrary units (AU) normalized to total protein. Human asyn is not
972 expressed in the ***E,*** A1/C1 or ***F,*** the A2/C2 region, but is detectable in the ***G,*** A4 and ***H,***
973 A5 regions of Tg mice by immunofluorescence. All data are from 3-mo old nTg and Tg
974 mice. Scale bar = 100μm (A, C) or 50 μm (E-H). Student's t-test ± SEM *p<0.05.
975
976 **Figure 4: DBH-hSNCA mice display age-dependent behavioral abnormalities**
977 **similar to the non-motor symptoms of PD. *A,*** 3-mo and 14-mo Tg mice have increased
978 sleep latencies. ***B,*** Tg mice display anxiety-like behavior by marble-burying test at 14-
979 mos and 24-mos and ***C,*** latency to re-enter the center in the open field test at 14-mos. ***D,***
980 There is a significant effect of genotype at 14-mos with Tg mice exhibiting significantly
981 more percent time freezing during fear training (center panel; bars represent tone
982 presentation, bolt represents foot shock) and ***E,*** contextual learning**.** ***F,*** There was no
983 effect of genotype in percent time freezing during cued test at any age. ***G,*** Ambulatory
984 behavior does not differ by genotype at any age. Students t-test of genotype ± SEM in A,
985 B & C. Repeated measures ANOVA ± SEM in D, E, F, and G. *p<0.05, ***p<0.001.
986
987 **Figure 5: Adrenergic receptor antagonists normalize sleep latency in 3- and 14-mo**
988 **old DBH-hSNCA mice. *A,*** The increased sleep latency observed in 3-mo, and ***B,*** 14-mo
989 old Tg mice was reduced by a cocktail of propranolol (β-adrenergic receptor antagonist)
990 and prazosin (α1-adrenergic receptor antagonist), while no effect was observed in nTg
991 mice at either age. Two-way ANOVA ± SEM. *p<0.05, **p<0.01.
992
993 **Figure 6: DBH-hSNCA LC neurons contain oligomeric and conformation-specific**
994 **asyn. *A,*** Representative images of oligomerized asyn (red) in LC neurons of (TH; green)
995 24-mos Tg mice as determined by proximity ligation assay (PLA). ***B***, Quantification of
996 PLA puncta demonstrated significantly more oligomerized asyn (red) in LC neurons of Tg

997 mice. ***C,*** Dot blot analysis of conformation-specific asyn and TH in the LC from 3-mo old
998 nTg and Tg mice and in brain tissue from SNCA knock-out and M83$^{+/+}$ asyn transgenic
999 mice. ***D*** Quantification of MJFR14 and TH expression normalized to total protein from dot
1000 blots. Conformation-specific asyn trended to negatively correlate to TH in the LC of nTg
1001 and Tg mice. ***E,*** Representative microphotographs of DAB-immunostained LC sections
1002 from 24-mo old mice and positive control tissue from an aged M83$^{+/+}$ asyn transgenic
1003 mouse with conformation-specific asyn (MJFR14). ***F***, Semi-quantification analysis of
1004 MJFR14 intensity. ***G***, Representative DAB-immunostained LC sections from 24-mo old
1005 mice and hippocampal positive control tissue from 6-mo old M20$^{+/-}$ asyn transgenic mice
1006 after brain inoculation with human asyn pre-formed fibrils (hPFF) to seed asyn inclusions
1007 with antibodies against pSer129 asyn (EP1536Y and LS4-2G12). Scale bar (hAsyn) =
1008 15µm. Scale bar (pser129 and MJFR14) = 100 µm. Student's t-test ± SEM. *p<0.05.
1009
1010 **Figure 7: Human asyn expression in LC neurons impacts striatal dopamine**
1011 **metabolism in aged DBH-hSNCA mice.** Catecholamine and catecholamine metabolite
1012 tissue content from hippocampus and striatum was measured by HPLC. ***A,*** Hippocampal
1013 NE is not affected by genotype. ***B,*** Striatal NE is reduced at 24-mos but does not reach
1014 statistical significance. The NE metabolite MHPG to NE ratio does not differ at any age in
1015 the ***C,*** hippocampus, or ***D,*** striatum. Dopamine content is not affected at any age in ***E,***
1016 hippocampus, or ***F,*** striatum. ***G,*** The ratio of the DA metabolite DOPAC to DA is
1017 unaffected in the hippocampus ***H,*** but is significantly reduced in the striatum of Tg mice
1018 at 24-mos. Student's t-test of genotype for each age group ± SEM. *p<0.05.
1019
1020 **Figure 8: Human asyn expression does not affect LC integrity.** NET-expressing LC
1021 cell bodies (red) percent immunoreactivity (IR) does not differ by genotype at 3-, 14-, or
1022 24-mos. Student's t-test of mean IR by genotype for each age group, ***A,*** graphed as fold
1023 change Tg from nTg mean ± SEM. ***B,*** Representative images. Scale bar = 50µm, *p<0.05.
1024
1025 **Figure 9: Tyrosine hydroxylase levels are elevated in young DBH-hSNCA Tg mice.**
1026 Tyrosine hydroxylase (TH: green) immunoreactivity is increased in LC neurons (NET: red)
1027 at 3- and 14-mos of age. ***A,*** Representative immunofluorescent images. ***B***, TH IR mean
1028 normalized to NET IR mean and expressed as fold change Tg from nTg mean % IR ±
1029 SEM. ***C,*** Western blot analysis of 3-mo old LC neurons confirms increased TH
1030 abundance. Data graphed as arbitrary densitometric units (AU) was normalized to total
1031 protein ± SEM. ***D,*** Representative western blot images of TH (top) and total protein stain
1032 (bottom). Student's t-test of nTg and Tg at each age, n=5-10. Scale bar = 50µm. *p<0.05.
1033
1034 **Fig 10. Human asyn in LC neurons affects expression of local inflammatory**
1035 **markers.** There are fewer Iba1-positive cells (red) in the LC (TH: green) at 14-mos. ***A,***
1036 Representative immunofluorescent images. ***B***, Microglial count in the LC graphed as fold
1037 change Tg from nTg Iba1+ cell count ± SEM. Student's t-test of nTg and Tg for each age
1038 group. Expression of astrocytic GFAP (red) is increased in the Tg LC (TH: green) at 24-
1039 mos of age. ***C,*** Representative immunofluorescent images. ***D***, Quantification of GFAP %
1040 IR in the LC as percent ROI graphed as fold change Tg IR from nTg mean IR ± SEM.
1041 Student's t-test of nTg and Tg for each age group. Scale bar = 50µm. *p<0.05.
1042

1043 **Fig 11: Hippocampal astrocytic GFAP expression is increased at 14-mos**. At 14-
1044 mos, Tg mice have significantly more GFAP (red) expression than nTg in the CA1 region
1045 of the hippocampus. Representative immunofluorescent images of ***A***, CA1, ***C,*** dentate
1046 gyrus, and ***E,*** CA3 regions. Quantification of GFAP IR as % area of ROI in ***B,*** CA1, ***D,***
1047 dentate gyrus, and ***F,*** CA3. Student's t-test of nTg and Tg for each age group, graphed
1048 as fold change Tg from nTg mean ± SEM. Scale bar = 50μm. *$p<0.05$.
1049
1050 **Fig 12: Fewer Iba1-expressing cells in hippocampal CA1 region in 14-mo old Tg**
1051 **DBH-hSNCA mice**. At 14-mos, Tg mice have fewer Iba1-expressing cells in hippocampal
1052 region CA1. ***A,*** Representative immunofluorescent images of Iba1-expressing cells (red).
1053 ***B,*** Quantification of Iba1-expressing cells in CA1 graphed as Tg fold change from nTg
1054 mean ± SEM. Student's t-test by genotype for each age group. Nuclear stain in blue.
1055 Scale bar = 150μm. *$p<0.05$.
1056
1057 **Figure 13: Asyn expression in LC neurons results in age-dependent degeneration**
1058 **of hippocampal LC fibers.** NET (red) IR is reduced in the dentate gyrus of Tg mice at
1059 24-mos. Representative immunofluorescent images of ***A***, CA1, ***C,*** dentate gyrus, and ***E,***
1060 CA3 regions. Quantification of NET IR as percent area of ROI in ***B,*** CA1, ***D,*** dentate gyrus,
1061 and ***F,*** CA3. Student's t-test of nTg and Tg for each age group, graphed as fold change
1062 Tg from nTg mean ± SEM. Scale bar = 150μm. *$p<0.05$.
1063
1064 **Figure 14: Proposed model of human asyn effects on noradrenergic**
1065 **neurotransmission**. Human asyn may enhance extracellular NE by several
1066 mechanisms. #1 – Increased expression of asyn could potentiate clustering of synaptic
1067 vesicles at the presynaptic membrane. #2 – Elevated asyn expression could reduce
1068 norepinephrine transporter (NET) expression at the plasma membrane. #3 – asyn
1069 modulation of L-type voltage gated calcium channels could enhance neuronal excitability.
1070 #4 – human asyn expression could enlarge the size of and slow the closing of vesicular
1071 fusion pores, allowing more NE to spill into the extracellular space.
1072
1073

Figure 1

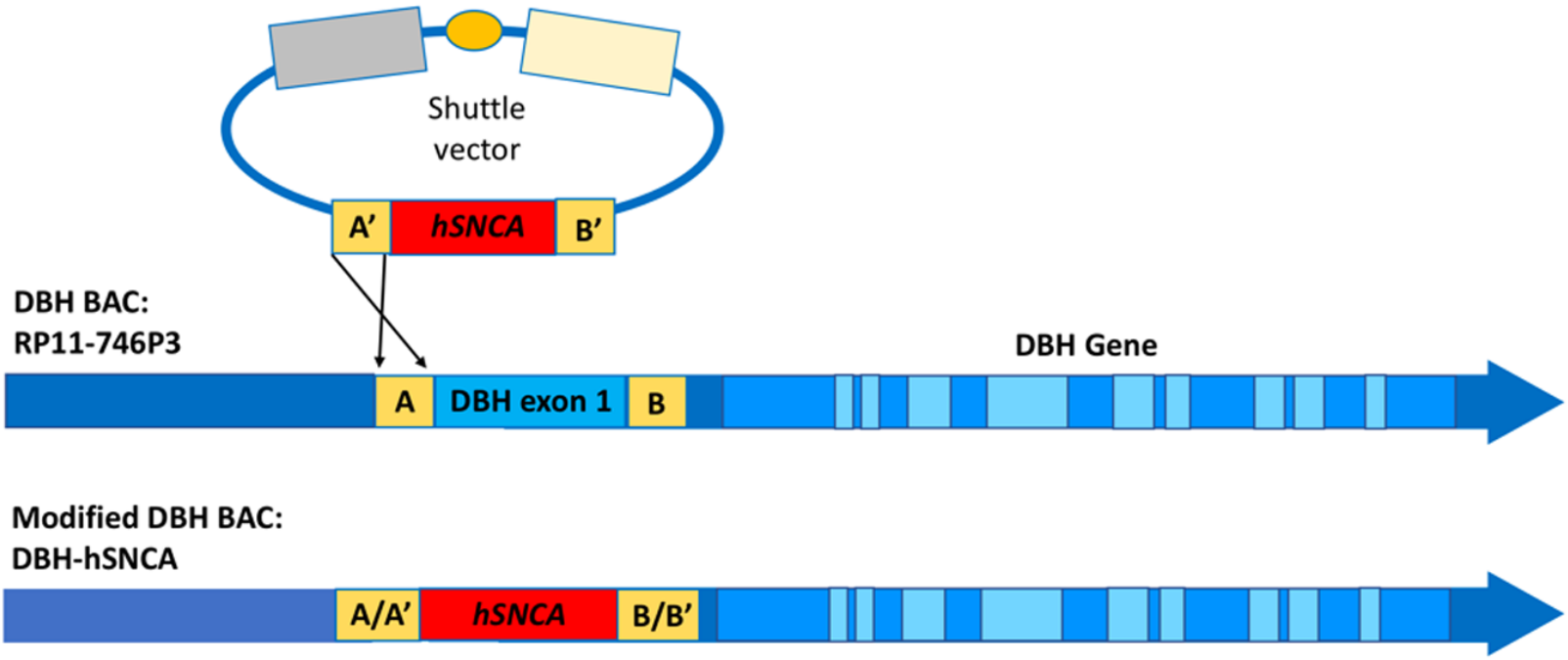
Shuttle
vector
A'
hSNCA
B'
DBH BAC:
RP11-746P3
DBH Gene
A
DBH exon 1
B
Modified DBH BAC:
DBH-hSNCA
A/A'
hSNCA
B/B'

Figure 2

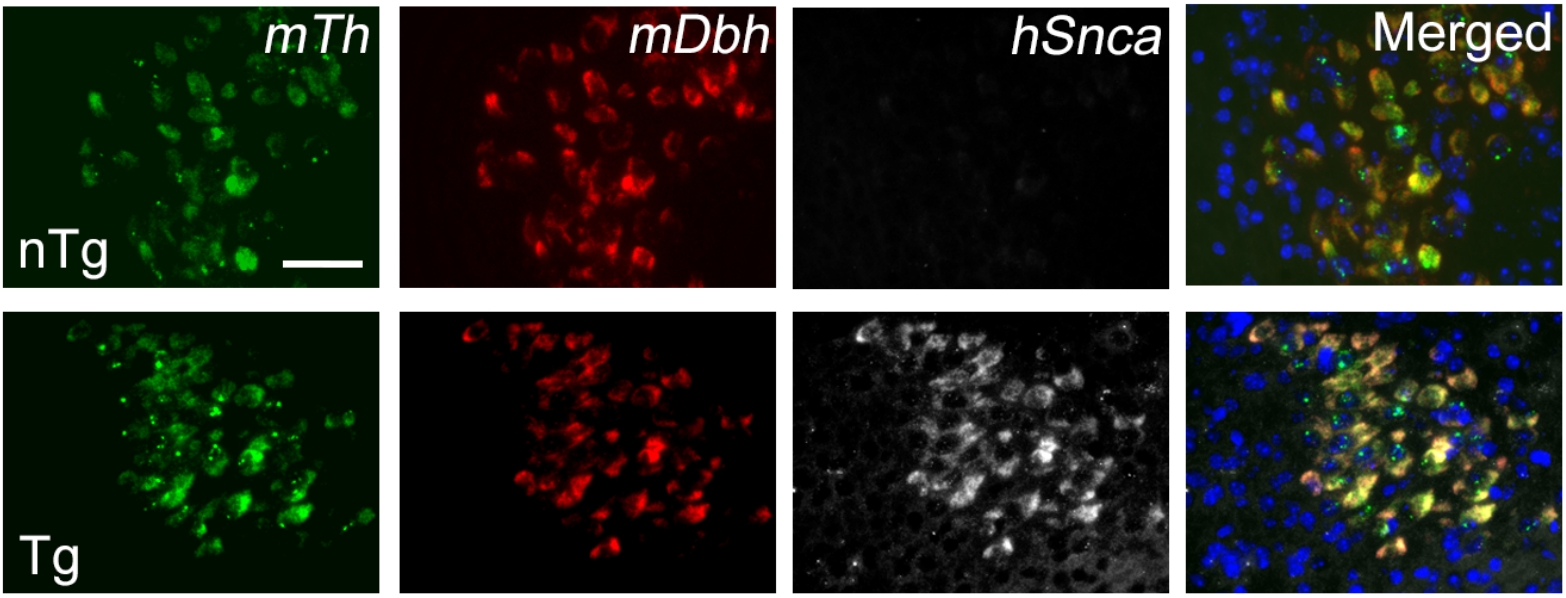

Figure 3

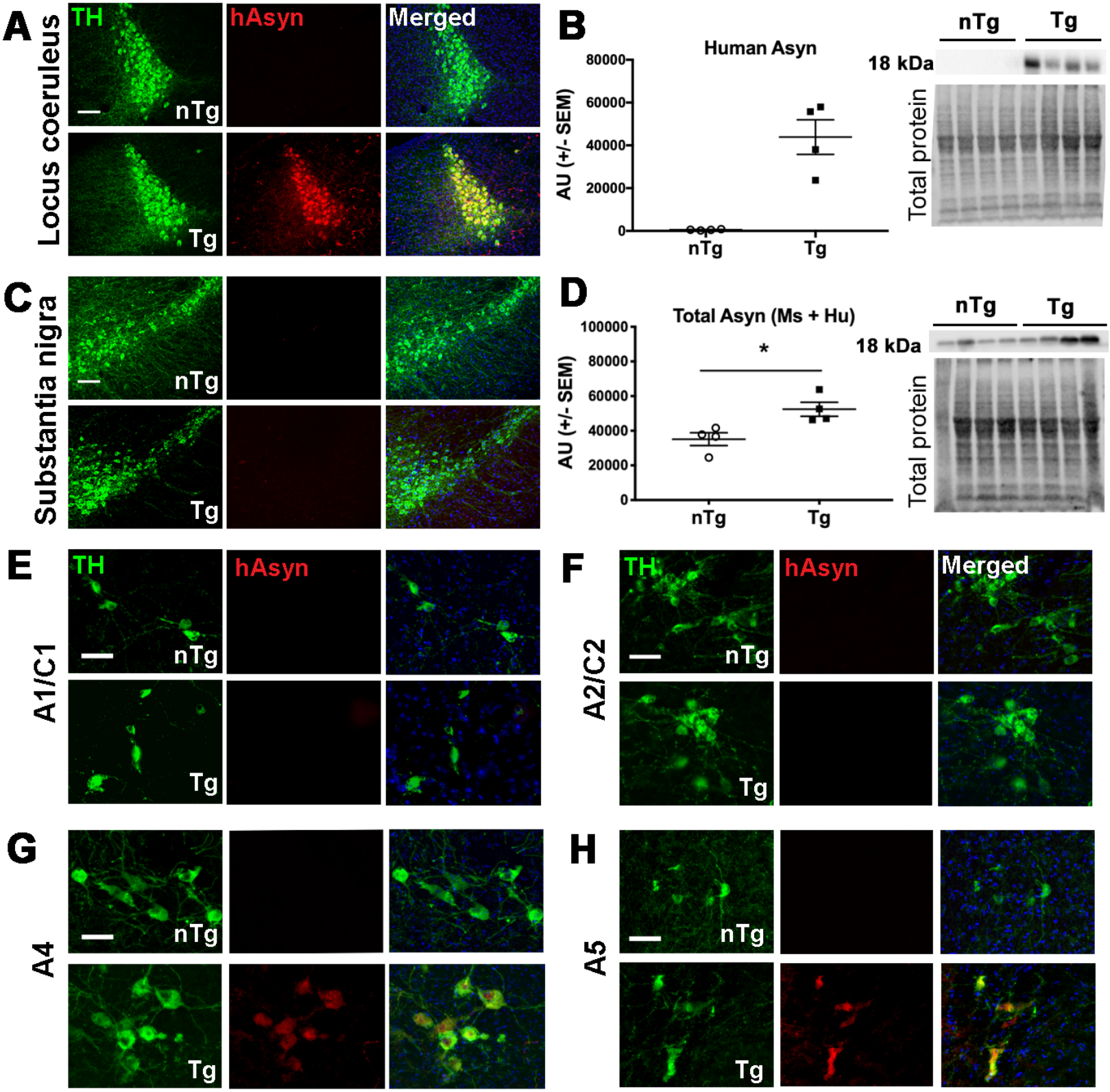
A
Locus coeruleus
TH
hAsyn
Merged
nTg
Tg
B
Human Asyn
AU (+/- SEM)
80000
60000
40000
20000
0
nTg
Tg
18 kDa
Total protein
C
Substantia nigra
D
Total Asyn (Ms + Hu)
100000
*
E
A1/C1
F
A2/C2
G
A4
H
A5

Figure 4

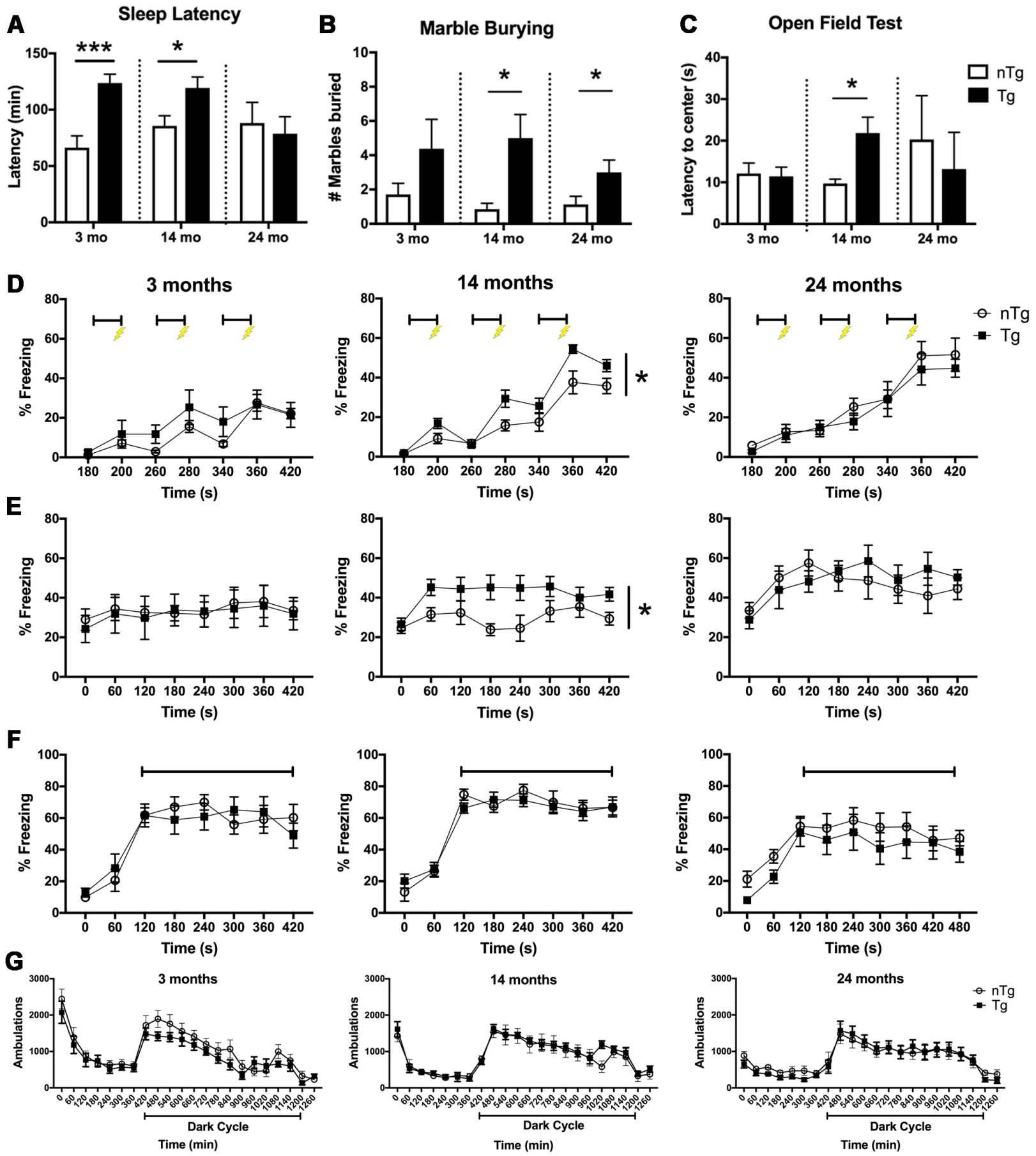
A
Sleep Latency
Latency (min)
***
*
3 mo
14 mo
24 mo
B
Marble Burying
Marbles buried
*
*
C
Open Field Test
Latency to center (s)
*
nTg
Tg
D
3 months
14 months
24 months
% Freezing
Time (s)
E
F
G
Ambulations
Dark Cycle
Time (min)

Figure 5

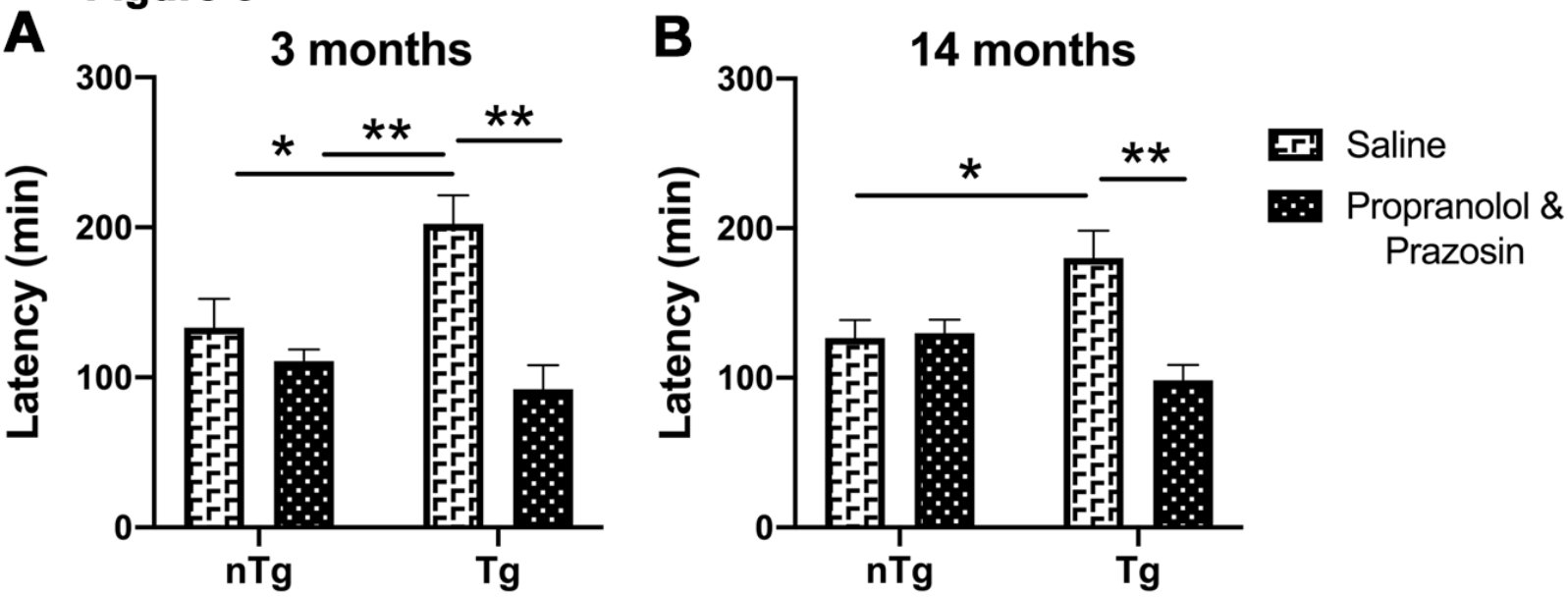
A
3 months
Latency (min)
300
200
100
0
*
**
**
nTg
Tg
B
14 months
Latency (min)
300
200
100
0
*
**
nTg
Tg
Saline
Propranolol &
Prazosin

Figure 6

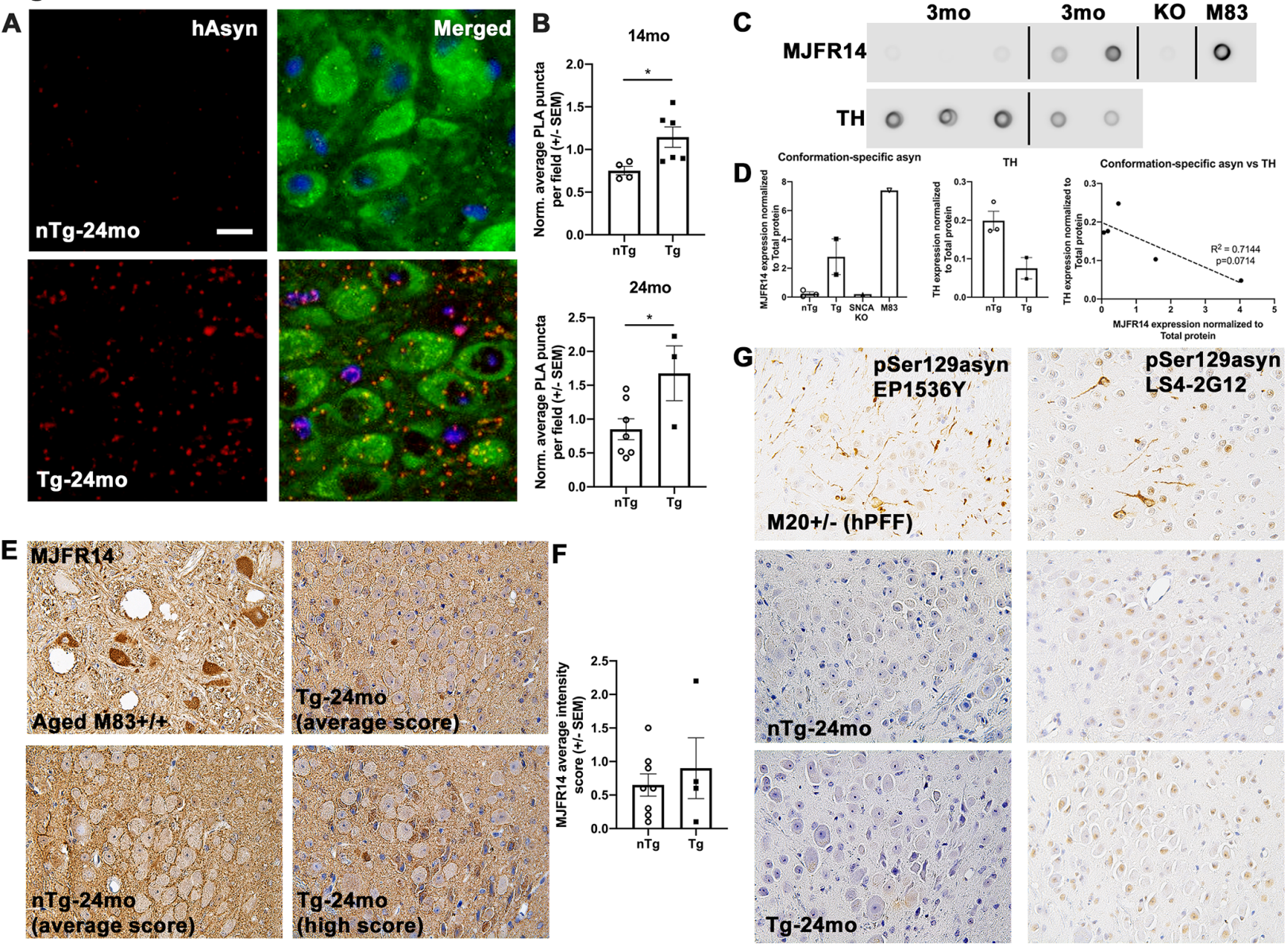
A
hAsyn
Merged
nTg-24mo
Tg-24mo
B
14mo
Norm. average PLA puncta per field (+/- SEM)
nTg
Tg
24mo
C
nTg 3mo
Tg 3mo
SNCA KO
M83
MJFR14
TH
D
Conformation-specific asyn
TH
Conformation-specific asyn vs TH
MJFR14 expression normalized to Total protein
TH expression normalized to Total protein
SNCA KO
R2 = 0.7144
p=0.0714
E
MJFR14
Aged M83+/+
Tg-24mo (average score)
nTg-24mo (average score)
Tg-24mo (high score)
F
MJFR14 average intensity score (+/- SEM)
G
pSer129asyn EP1536Y
pSer129asyn LS4-2G12
M20+/- (hPFF)
nTg-24mo
Tg-24mo

Figure 7

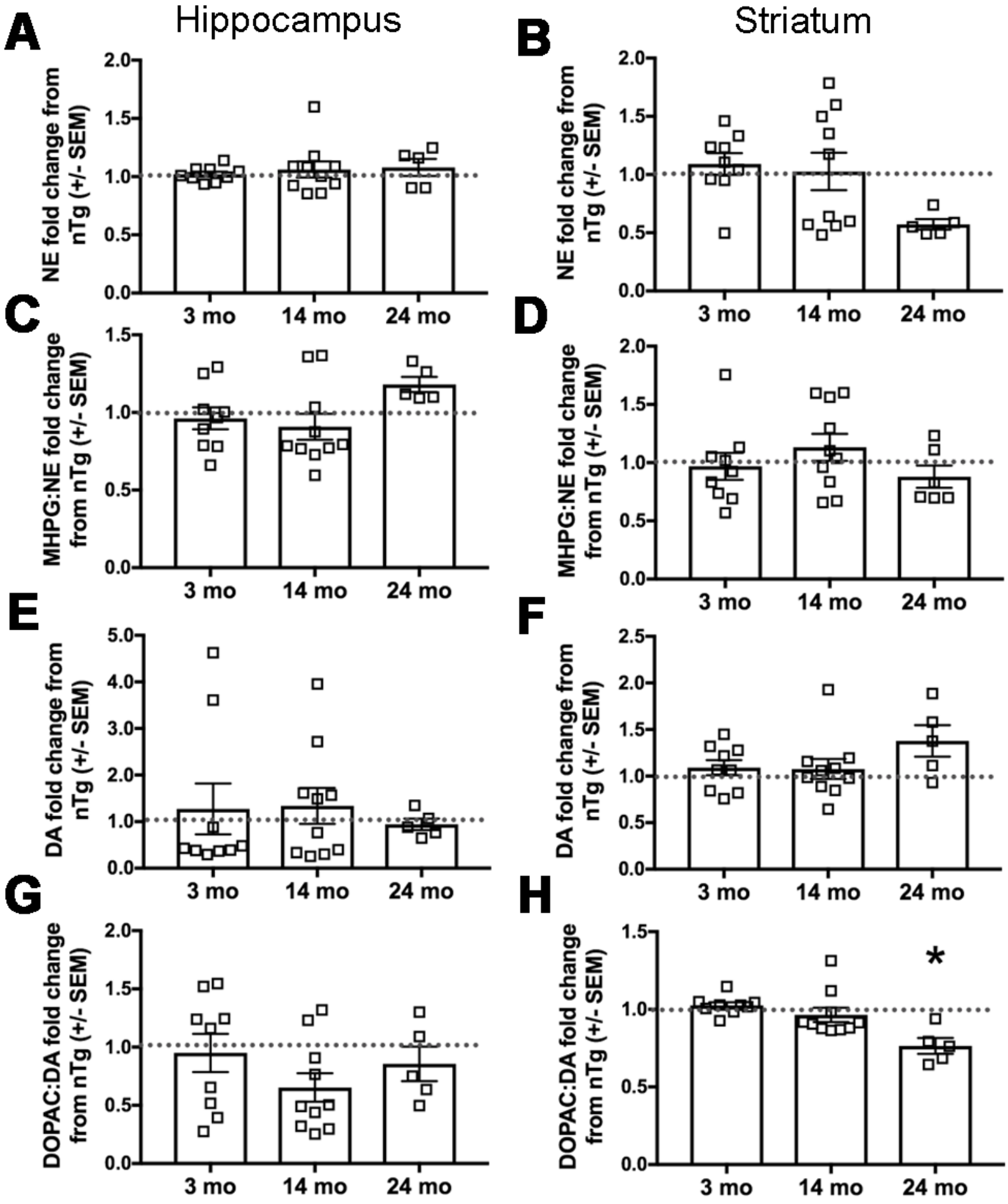
A
Hippocampus
B
Striatum
NE fold change from nTg (+/- SEM)
2.0
1.5
1.0
0.5
0.0
3 mo
14 mo
24 mo
C
D
MHPG:NE fold change from nTg (+/- SEM)
1.5
1.0
0.5
0.0
E
F
DA fold change from nTg (+/- SEM)
5.0
4.0
3.0
2.0
1.0
0.0
2.5
G
H
DOPAC:DA fold change from nTg (+/- SEM)
*

Figure 8

A

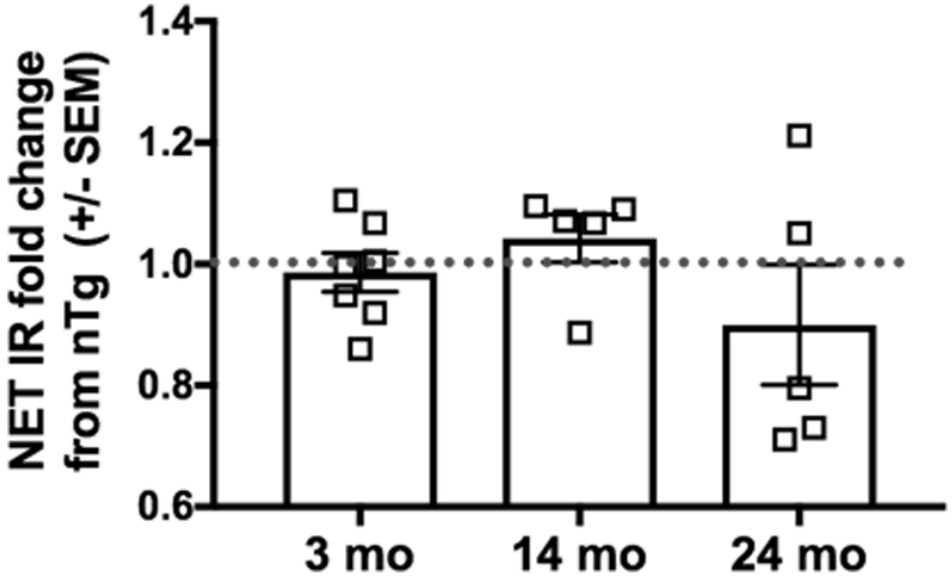
NET IR fold change
from nTg (+/- SEM)
1.4
1.2
1.0
0.8
0.6
3 mo
14 mo
24 mo

B

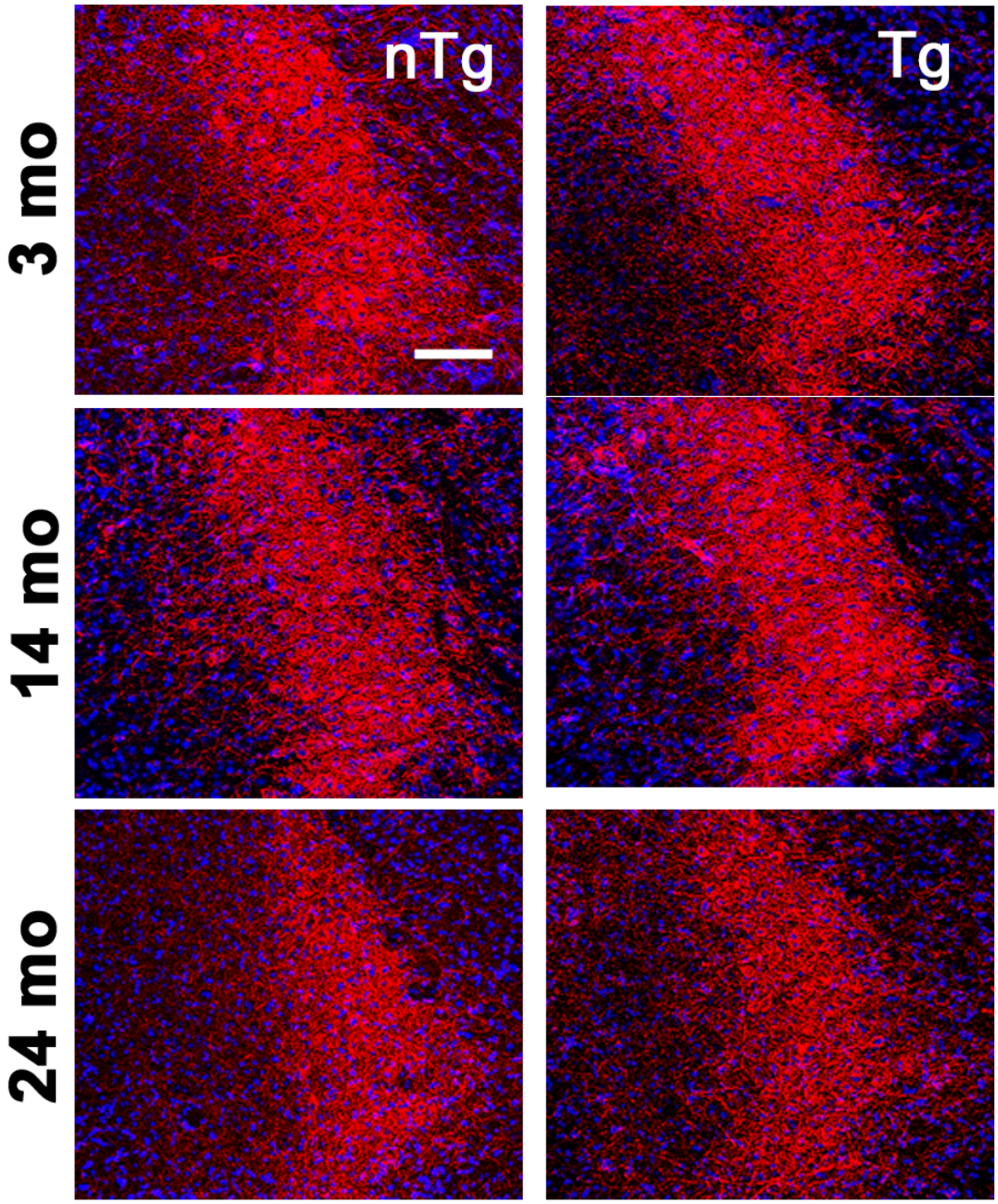
nTg
Tg
3 mo
14 mo
24 mo

Figure 9

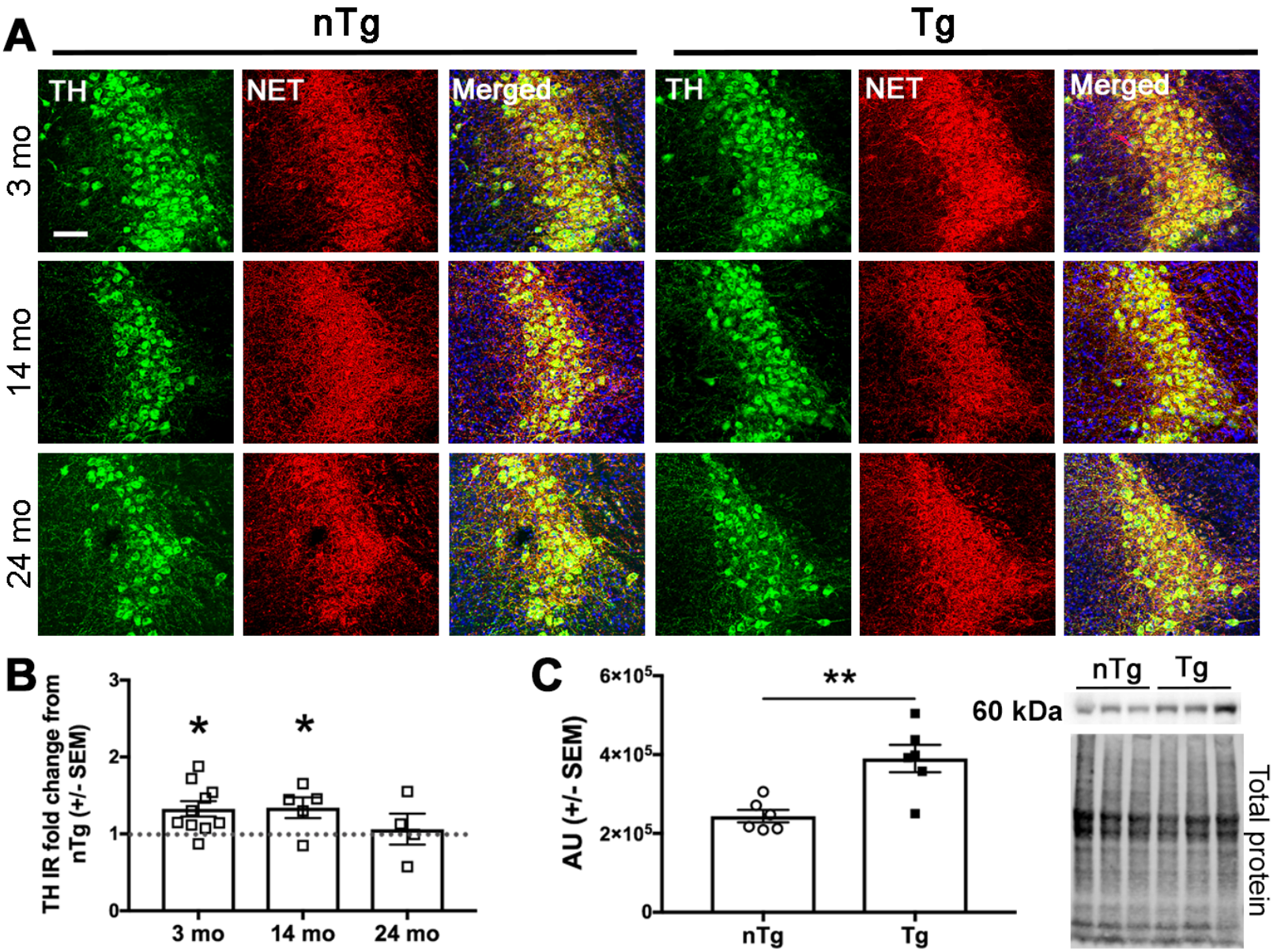
A
nTg
Tg
TH
NET
Merged
3 mo
14 mo
24 mo
B
TH IR fold change from nTg (+/- SEM)
3
2
1
0
*
*
3 mo
14 mo
24 mo
C
AU (+/- SEM)
6×10^5
4×10^5
2×10^5
0
**
nTg
Tg
60 kDa
Total protein

Figure 10

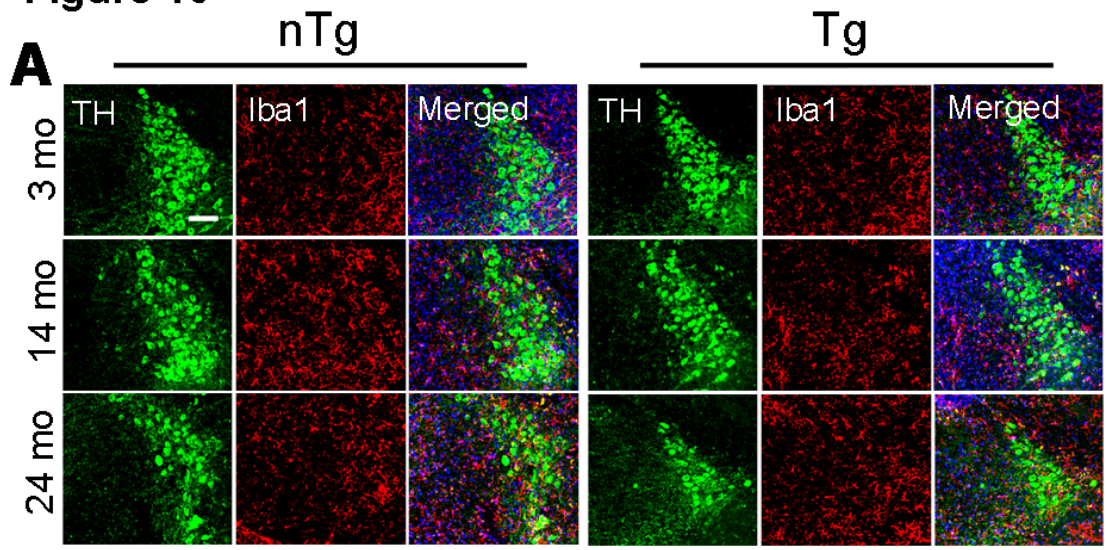
A
nTg
Tg
TH
Iba1
Merged
3 mo
14 mo
24 mo

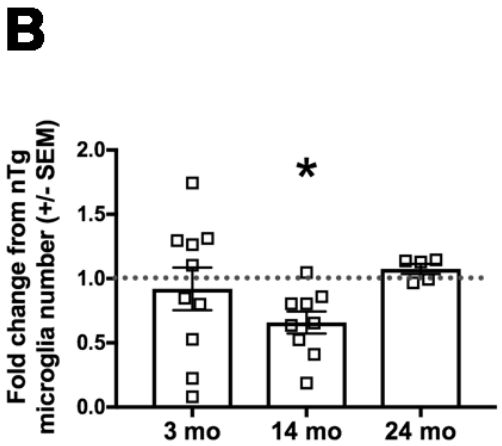
B
Fold change from nTg microglia number (+/- SEM)
2.0
1.5
1.0
0.5
0.0
*
3 mo
14 mo
24 mo

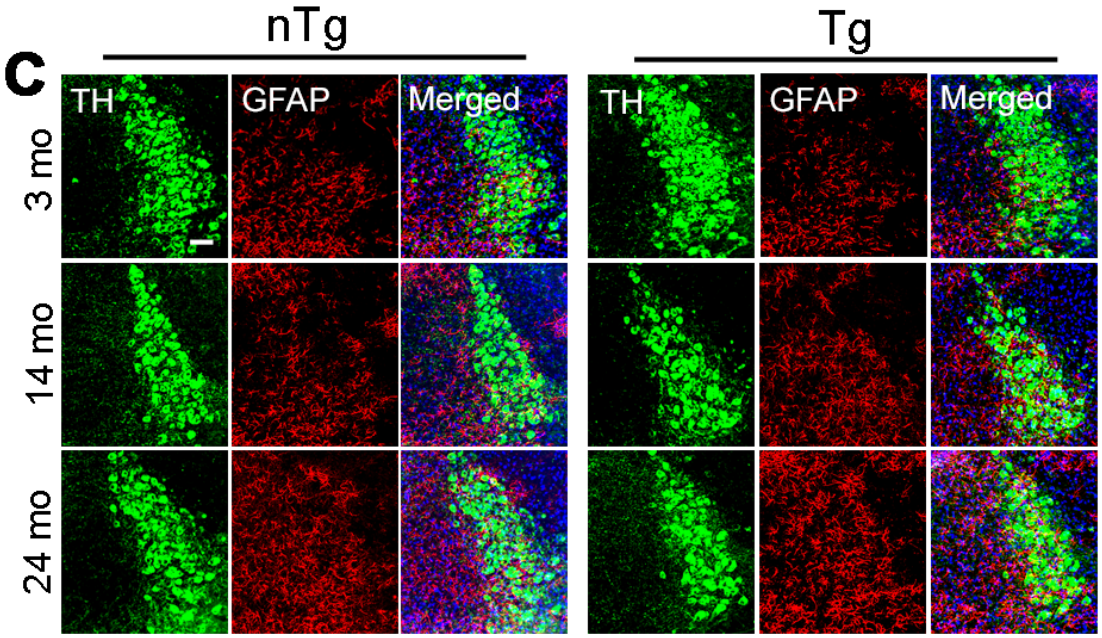
C
nTg
Tg
TH
GFAP
Merged
3 mo
14 mo
24 mo

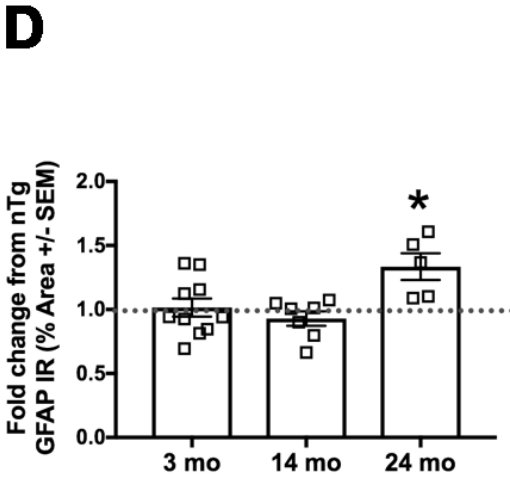
D
Fold change from nTg GFAP IR (% Area +/- SEM)
2.0
1.5
1.0
0.5
0.0
*
3 mo
14 mo
24 mo

Figure 11

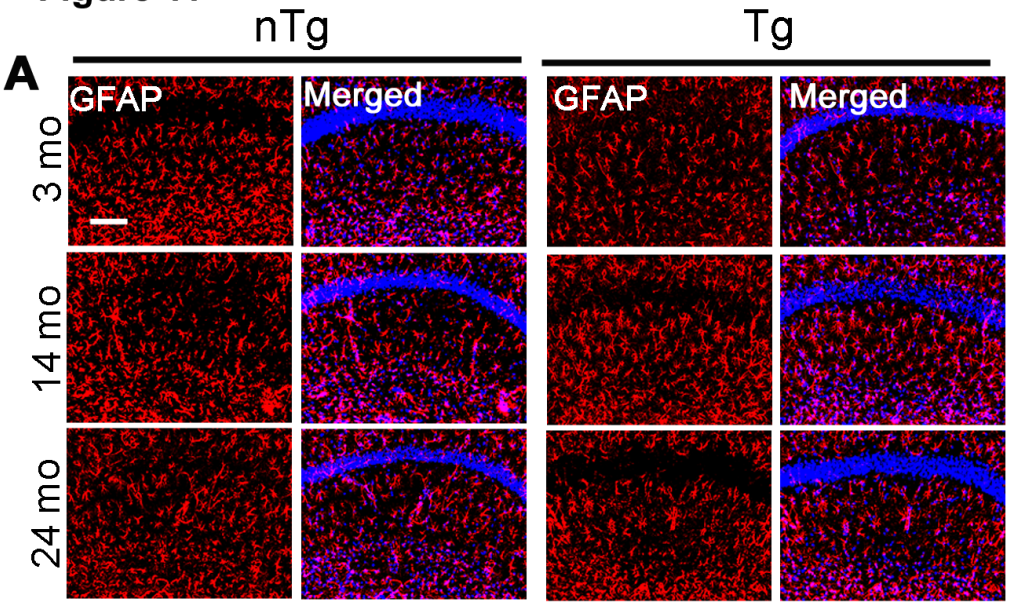
A
nTg
Tg
GFAP
Merged
GFAP
Merged
3 mo
14 mo
24 mo

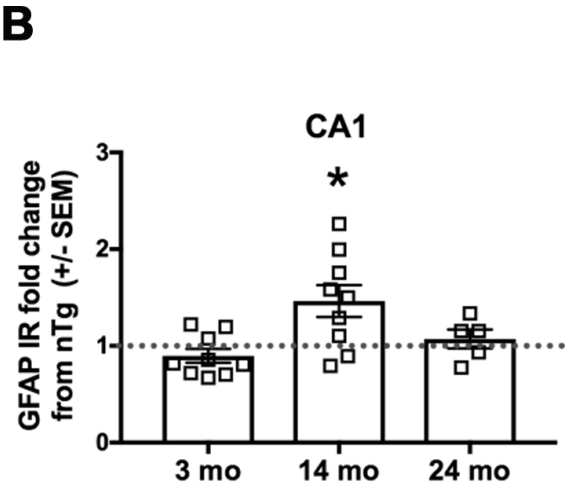
B
CA1
GFAP IR fold change from nTg (+/- SEM)
0
1
2
3
*
3 mo
14 mo
24 mo

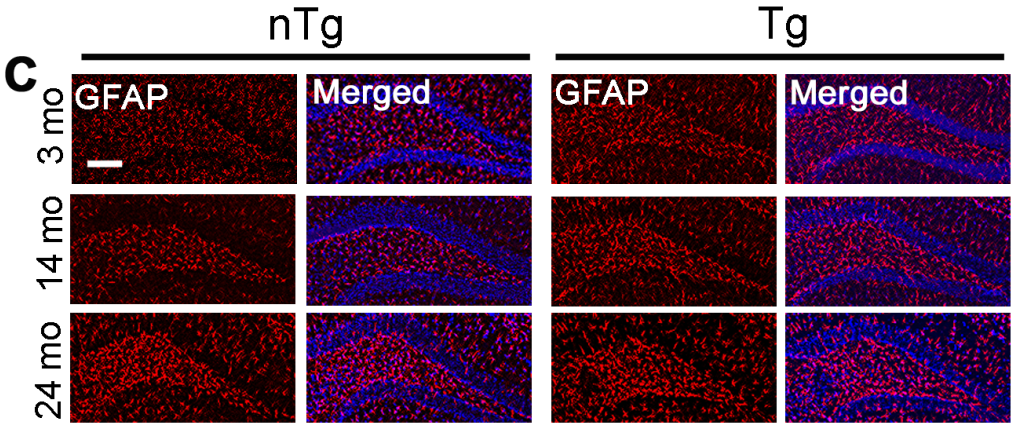
C
nTg
Tg
GFAP
Merged
GFAP
Merged
3 mo
14 mo
24 mo

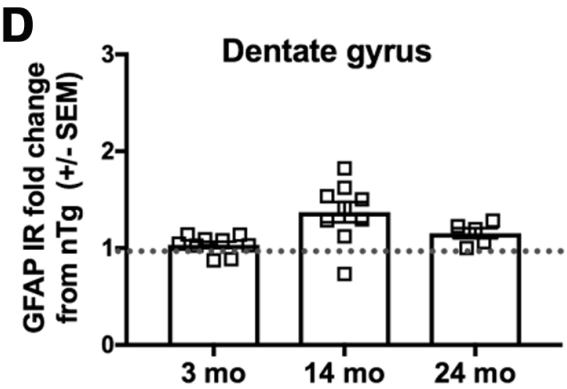
D
Dentate gyrus
GFAP IR fold change from nTg (+/- SEM)
0
1
2
3
3 mo
14 mo
24 mo

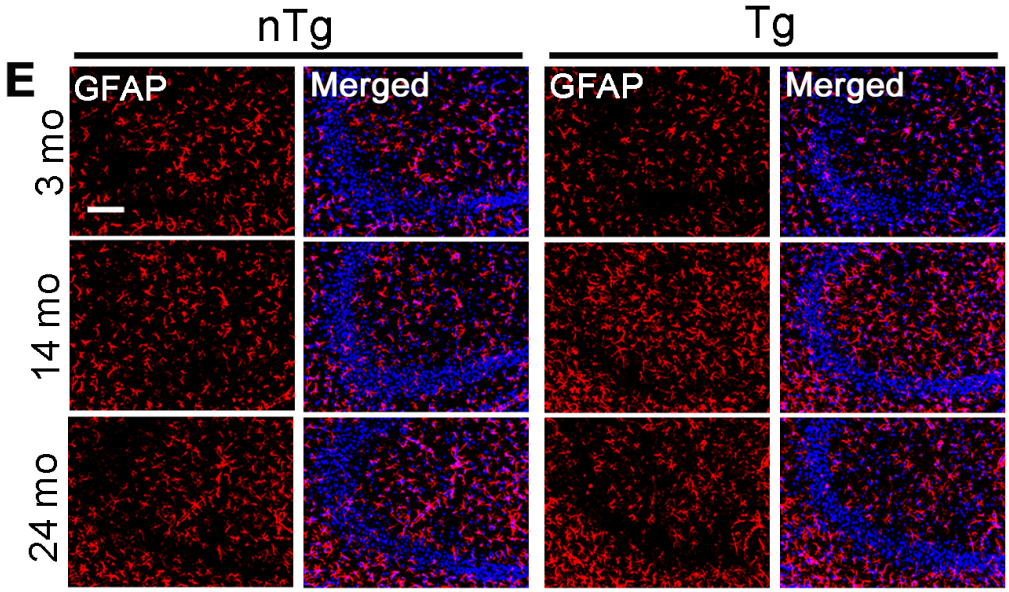
E
nTg
Tg
GFAP
Merged
GFAP
Merged
3 mo
14 mo
24 mo

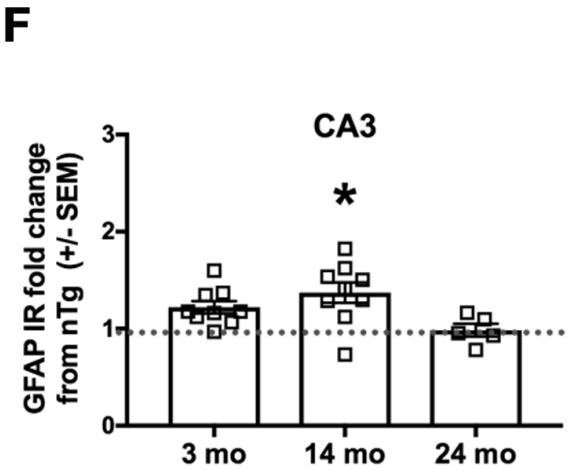
F
CA3
GFAP IR fold change from nTg (+/- SEM)
0
1
2
3
*
3 mo
14 mo
24 mo

Figure 12

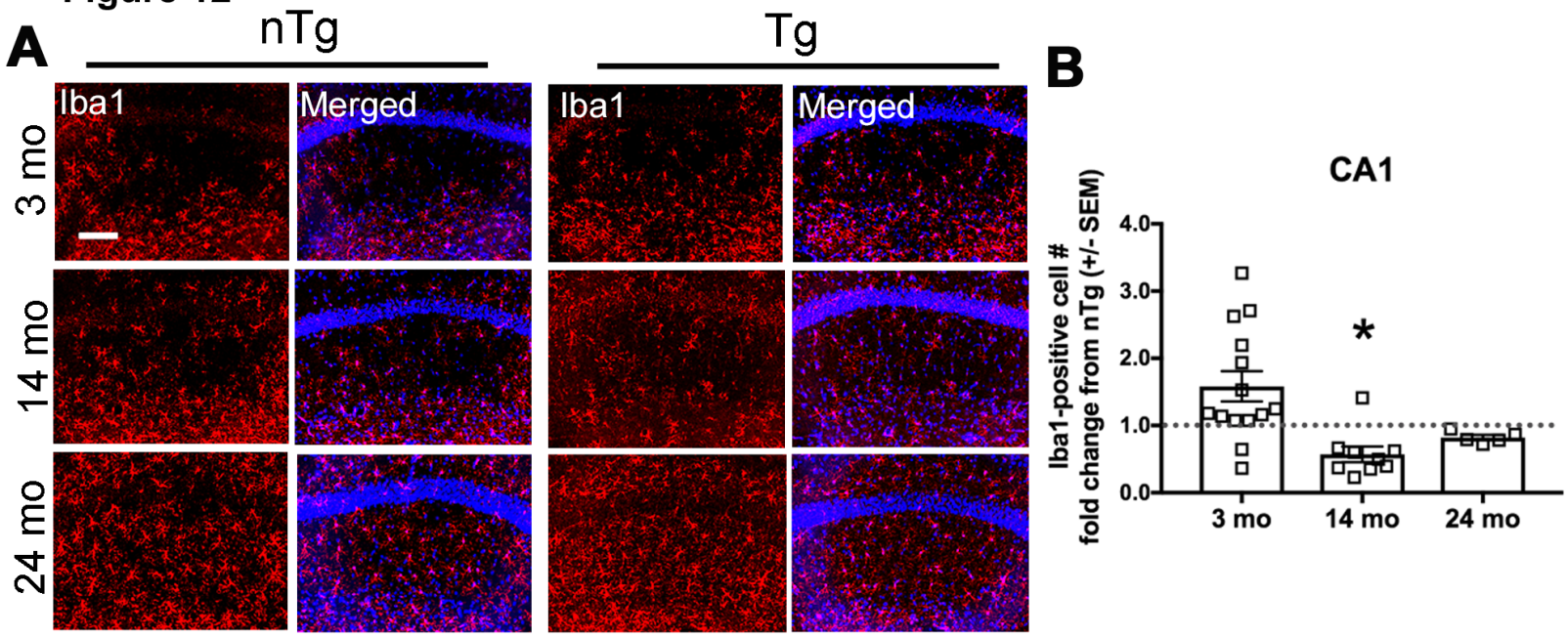
A
nTg
Tg
Iba1
Merged
Iba1
Merged
3 mo
14 mo
24 mo
B
CA1
Iba1-positive cell #
fold change from nTg (+/- SEM)
4.0
3.0
2.0
1.0
0.0
*
3 mo
14 mo
24 mo

Figure 13

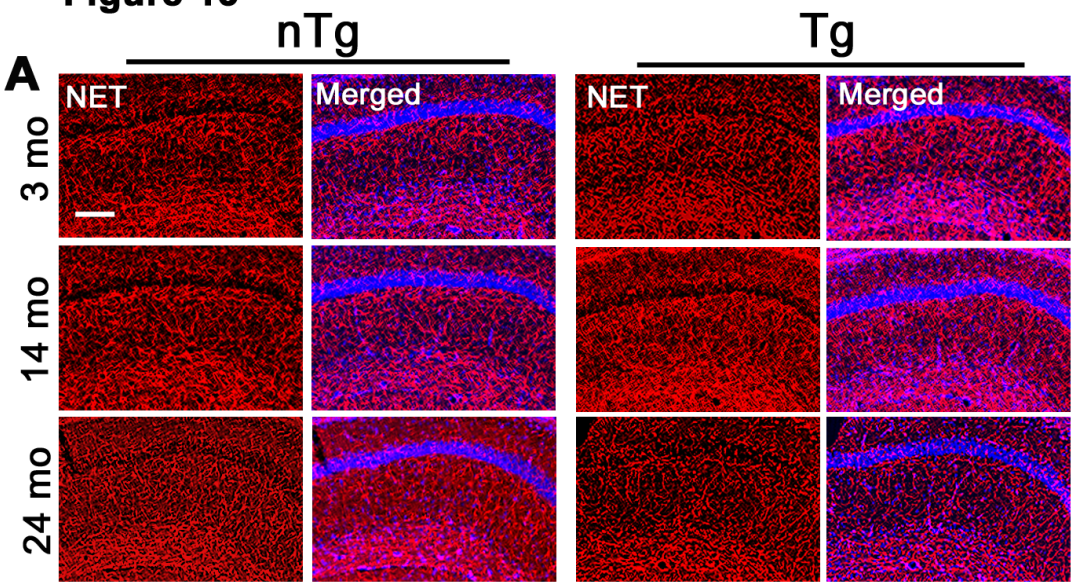
A
nTg
Tg
NET
Merged
NET
Merged
3 mo
14 mo
24 mo

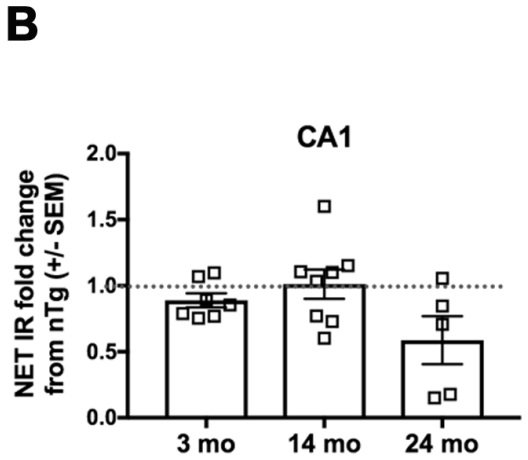
B
CA1
NET IR fold change from nTg (+/- SEM)
2.0
1.5
1.0
0.5
0.0
3 mo
14 mo
24 mo

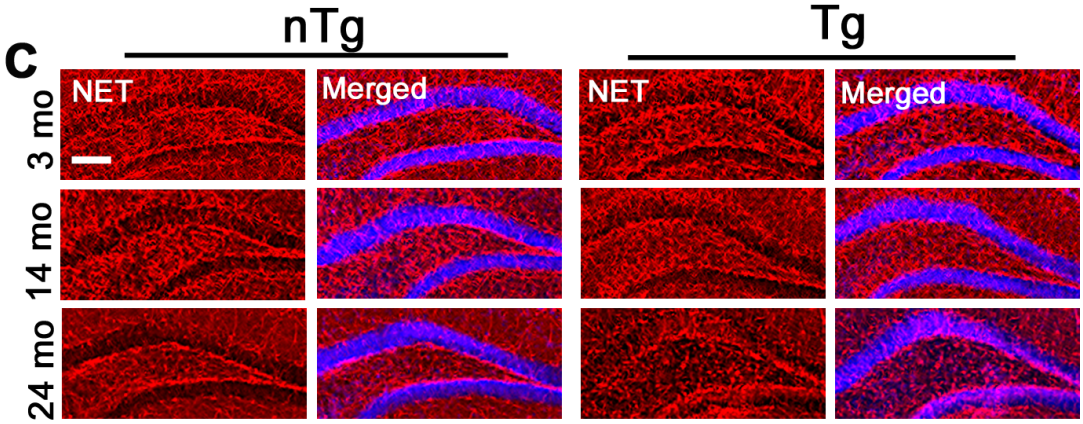
C
nTg
Tg
NET
Merged
NET
Merged
3 mo
14 mo
24 mo

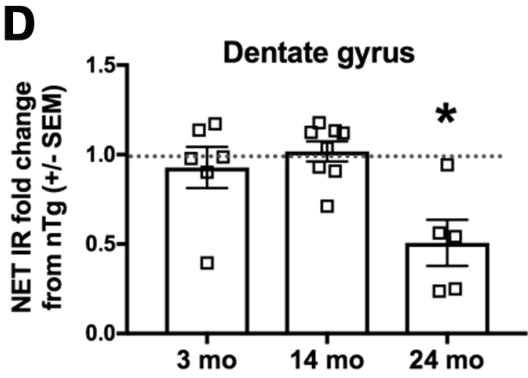
D
Dentate gyrus
NET IR fold change from nTg (+/- SEM)
1.5
1.0
0.5
0.0
*
3 mo
14 mo
24 mo

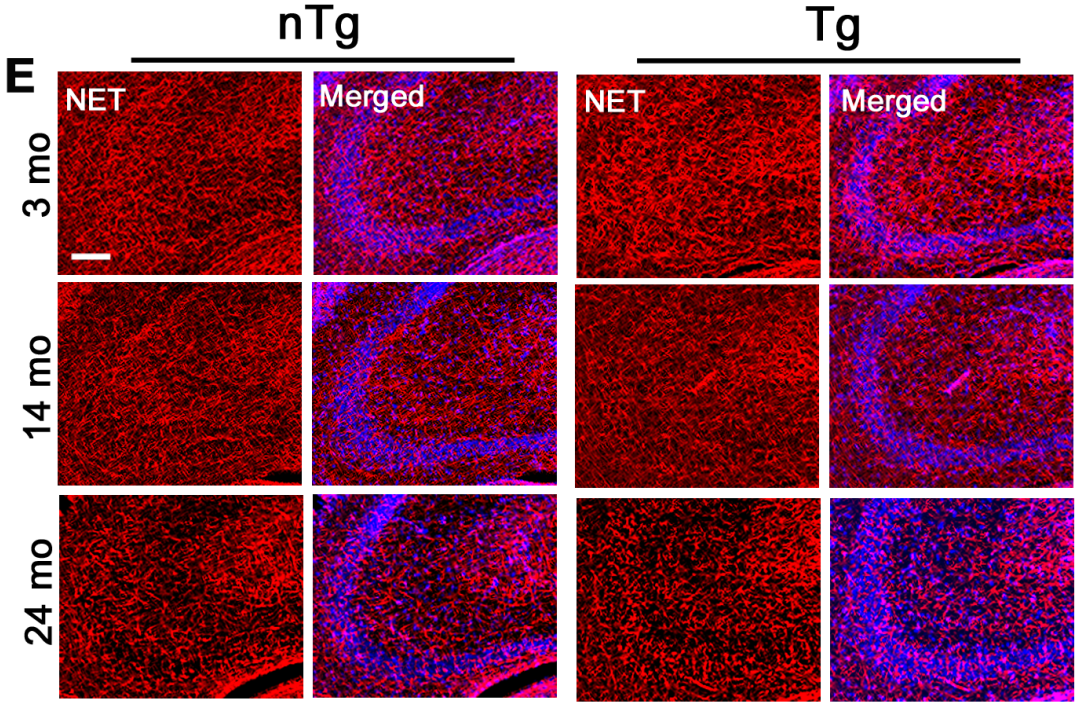
E
nTg
Tg
NET
Merged
NET
Merged
3 mo
14 mo
24 mo

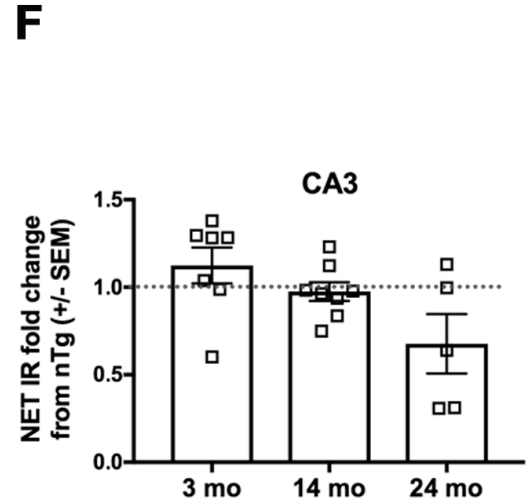
F
CA3
NET IR fold change from nTg (+/- SEM)
1.5
1.0
0.5
0.0
3 mo
14 mo
24 mo

Figure 14

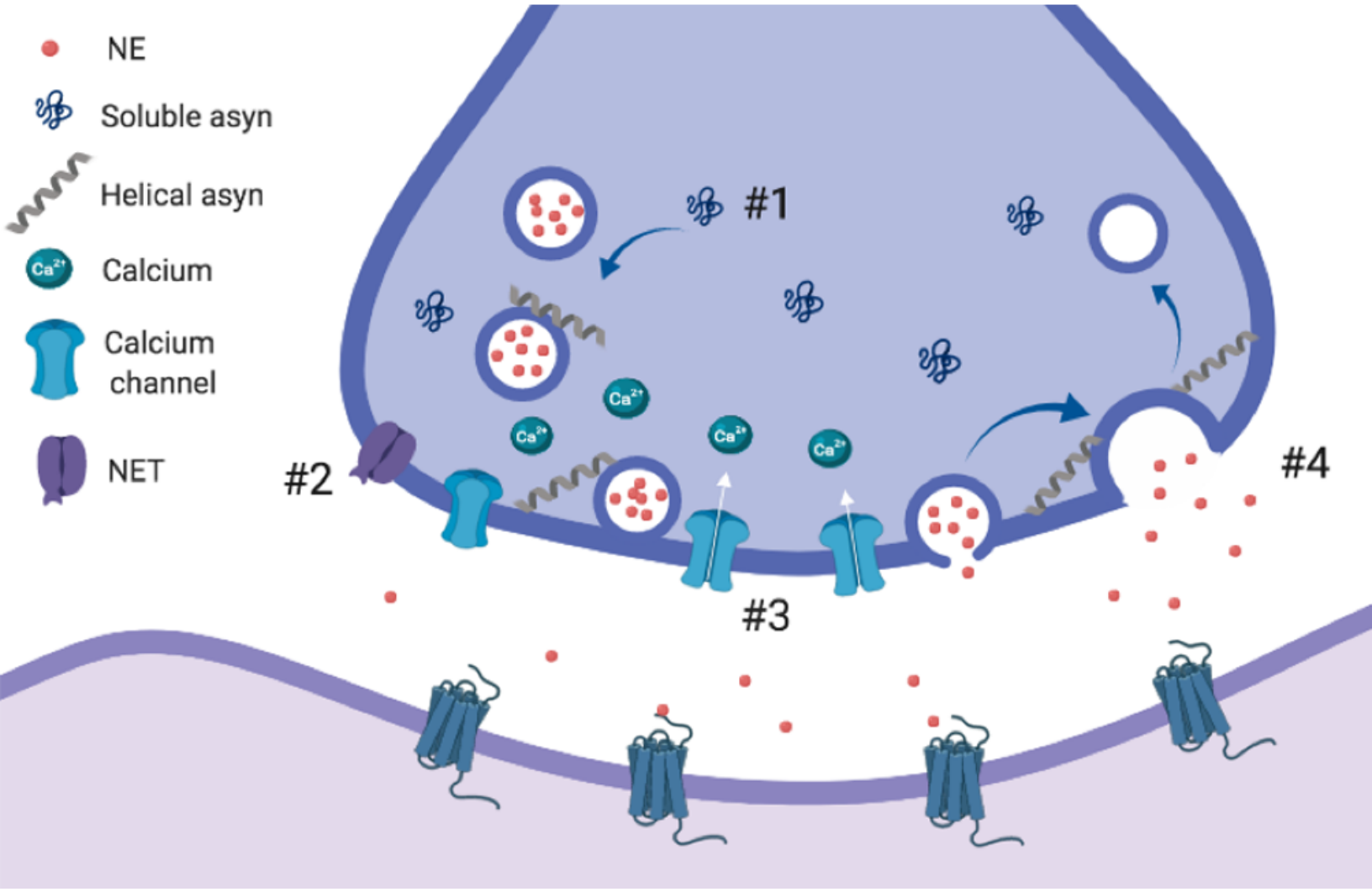
NE
Soluble asyn
Helical asyn
Calcium
Calcium channel
NET
#1
#2
#3
#4

Table 1: Primary and secondary antibodies used in these studies

Immunofluorescence

Antigen	Host	Manufacturer	Cat. No.	Dilution
α-synuclein (Hu)	Mouse	Biolegend	807801	1:500
DAT	Rat	Millipore	MAB369	1:500
GFAP	Rabbit	Zymed	13-0300	1:500
Iba1	Rabbit	Wako	019-19741	1:500
NET	Mouse	Mab Technologies	NET05-2	1:1,000
Tyrosine hydroxylase	Rabbit	Millipore	AB152	1:1,000
Tyrosine hydroxylase	Chicken	Abcam	AB76442	1:1,000
Anti-chicken AlexaFluor488	Goat	Invitrogen	A11039	1:1,000
Anti-rabbit AlexaFluor488	Goat	Invitrogen	A11015	1:1,000
Anti-mouse AlexaFluor594	Goat	Invitrogen	A11020	1:1,000
Anti-rabbit AlexaFluor594	Goat	Invitrogen	A11012	1:1,000
Anti-rat AlexaFluor594	Goat	Invitrogen	A11007	1:1,000

Proximity ligation assay

Antigen	Host	Manufacturer	Cat. No.	Dilution
α-synuclein (Hu)	Mouse	Abcam	AB80627	1:1000

Immunoblotting

Antigen	Host	Manufacturer	Cat. No.	Dilution
α-synuclein (Hu)	Mouse	Abcam	AB80627	1:1,000
α-synuclein (Ms + Hu)	Rabbit	Santa Cruz	SC-7011R	1:500
Tyrosine hydroxylase	Rabbit	Millipore	AB152	1:1,000
Anti-mouse HRP	Goat	Jackson ImmunoResearch	115-036-072	1:1,000
Anti-rabbit HRP	Goat	Jackson ImmunoResearch	111-036-047	1:1,000

IHC and Dot blot

Antigen	Host	Manufacturer	Cat. No.	Dilution
α-synuclein-pSer129 (EP1536Y)	Rabbit	Abcam	AB51253	1:2,500
α-synuclein-pSer129 LS4-2G12)	Mouse	*N.J. Rutherford et. al., 2016*		1:5,000
α-synucleni-conformation-specific	Rabbit	Abcam	AB209538	1:10,000 (IHC)
α-synucleni-conformation-specific	Rabbit	Abcam	AB209538	1:1,000 (dot blot)
Tyrosine hydroxylase	Rabbit	Millipore	AB152	1:500
Biotinylated anti-rabbit	Goat	Vector	BA-1000	1:200
Biotinylated anti-mouse	Horse	Vector	BA-2000	1:200
Anti-rabbit HRP	Goat	Jackson Immunoresearch	111-036-047	1:1,000